# GW190521 as a Highly Eccentric Black Hole Merger

V. Gayathri,[1] J. Healy,[2] J. Lange,[2] B. O'Brien,[1] M. Szczepańczyk,[1] I. Bartos,[1,*] M. Campanelli,[2] S. Klimenko,[1] C. Lousto,[2] and R. O'Shaughnessy[2,†]

[1]*Department of Physics, University of Florida, PO Box 118440, Gainesville, FL 32611-8440, USA*
[2]*Center for Computational Relativity and Gravitation, Rochester Institute of Technology, Rochester, NY 14623, USA*

The stellar-mass black hole merger GW190521 is the heaviest system discovered by LIGO/Virgo so far, with masses unexpected from stellar evolution. The system underwent precession due to its black hole spin orientation, a signature of binaries formed through gravitational capture. Capture through close encounters can also lead to eccentric binary orbits, but this feature is currently difficult to identify due to the lack of suitable gravitational waveforms. No eccentric merger has been reported to date. Here we show that GW190521 is the most consistent with a highly eccentric black hole merger. We carried out 325 numerical relativity simulations to generate an effective $\sim 3 \times 10^4$ gravitational waveforms to compare to the observed data, much greater than previously available at high eccentricities. We find that GW190521 is best explained by a high-eccentricity, precessing model with $e \approx 0.7$. All properties of GW190521 point to its origin being the repeated gravitational capture of black holes, making GW190521 the first of LIGO/Virgo's discoveries whose formation channel is identified.

## I. INTRODUCTION

As the LIGO [1] and Virgo [2] observatories are rapidly increasing the number of discovered black hole mergers, the origin of these mergers is still uncertain. The discovery of GW190521 is a milestone in resolving the question of origin [3, 4]. With a total mass of $142^{+28}_{-16}$, at least one of the black holes of this binary is inconsistent with our understanding of stellar evolution, as pair-instability in massive stars limits the remnant black hole's mass at $\lesssim 65\,\mathrm{M}_\odot$. An alternate origin is required. The most plausible explanation is that the black holes in GW190521 were forged in previous mergers of smaller black holes [5–7].

Such a black hole assembly through consecutive mergers can occur in environments with a high number density of black holes, such as galactic nuclei, in which chance encounters between black holes is common, and in which the newly formed black holes are unable to escape from the system.

An observational signature of chance encounters is orbital eccentricity [8–11]. As black holes borne into a binary will orbit each other for billions of years, their orbital eccentricity will diminish through the emission of gravitational waves. Binaries formed through gravitational capture in chance encounters, on the other hand, can form with small orbital radii and high initial eccentricity, leaving insufficient time for the binary to lose its eccentricity before emitting gravitational waves at frequencies to which LIGO/Virgo is sensitive. Alternatively, interaction of an existing binary with nearby black holes can also increase its eccentricity [12–17]. This possibility also arises in a dense black hole population.

Despite its importance, it is difficult to identify orbital eccentricity through observations [18–22]. Eccentricity expands the degrees of freedom of gravitational waveforms, making standard template-based searches problematic to carry out in practice. More fundamentally, there is currently no comprehensive waveform family for the full eccentric parameter space and current surveys[23] are limited to $e < 0.5$ and low black hole mass. As eccentric orbits combine close encounters with more distant, slower orbital evolution, they present complications both for waveform computations utilizing numerical relativity, and for those using post-Newtonian approximations [24].

In this paper we self-consistently analyzed the possibility and implications of GW190521 being an eccentric binary source. We carried out 325 numerical relativity simulations to produce a suite of binary merger gravitational waveforms that cover the full eccentricity range, including non-spinning, aligned-spin and spin-induced precessing waveforms (Sec. II). We estimated the binary properties of GW190521 using Bayesian parameter estimation through directly comparing our numerical-relativity simulations with gravitational-wave strain data using the RIFT package [25–28] (Sec. III). To determine whether our reconstructed binary properties correspond to a gravitational waveform that is an accurate explanation of the observed data, we quantitatively tested this consistency using the a model-independent waveform reconstruction algorithm (Sec. IV). We present our conclusions from these analyses in Sec. VI.

## II. NUMERICAL EVOLUTION

We carried out numerical relativity simulations of eccentric black hole mergers using the LazEv code [29], an implementation of the moving puncture approach [30]. We used the BSSNOK (Baumgarte-Shapiro-Shibata-Nakamura-Oohara-Kojima) family of evolution sys-

* imrebartos@ufl.edu
† rossma@rit.edu

tems [31–33]. All simulations used $6^{th}$ order spatial finite-differencing, $5^{th}$ order Kreiss-Oliger dissipation, and Courant factors of $1/3$ [34–36]. These techniques are the same used to generate quasicircular simulations [37–39], as our formalism is robust to deal with generic orbits.

The LazEv code uses the EinsteinToolkit [40, 41] / Cactus [42] / Carpet [43] infrastructure. The Carpet mesh refinement driver provides a "moving boxes" style of mesh refinement. In this approach, refined grids of fixed size are arranged about the coordinate centers of both holes. The code then moves these fine grids about the computational domain by following the trajectories of the two black holes.

To compute the numerical initial data, we used the puncture approach [44] along with the TwoPunctures [45] code. For each eccentric family, we first determined the initial separation and tangential quasicircular momentum, $p_{t,qc}$, that leads to a frequency of 10 Hz for a $30\,\mathrm{M}_\odot$ system, using the post-Newtonian techniques described in [46]. To increase the eccentricity of the system while keeping the initial data at an apocenter, the initial tangential momentum was modified by parameter, $0 < \epsilon < 1$, such that $p_t = p_{t,qc}(1-\epsilon)$. The eccentricity was then approximately $e = 2\epsilon/(1+\epsilon)$.

Gravitational waveforms were calculated via the radiative Weyl Scalar $\psi_4$, which was decomposed into $\ell$ and $m$ modes. We extracted the gravitational radiation at finite radius and extrapolated to $r = \infty$ using the perturbative extrapolation described in Ref. [47]. The gravitational strain waveform was then calculated from the extrapolated $\psi_4$ in Fourier space [48, 49].

We carried out 325 eccentric binary black hole simulations in this study, with eccentricities in the full $[0, 1]$ range. These simulations included non-spinning, aligned-spin and spin-precessing waveforms, and mass ratios $1/7 \leq q = m_2/m_1 \leq 1$. These gravitational waveforms were then scaled to correspond to different black hole masses, providing about 100 scaled mass values for each simulation. See the Supplementary Table for a detailed list of the parameters of the simulations.

## III. ESTIMATION OF BINARY PROPERTIES

Our numerical-relativity simulations were directly compared with gravitational-wave strain data using the RIFT package [25–28], assuming a Gaussian likelihood $\mathcal{L}(d|h)$. Here, $d$ is the recorded data, while $h$ is the time-dependent strain of the incoming gravitational wave signal. For each numerical-relativity simulation $\boldsymbol{\lambda}$, we calculated the marginal likelihood

$$\mathcal{L}_{\mathrm{marg}} = \max_{M_z} \int d\theta p(\theta) \mathcal{L}(d|h(\theta, \boldsymbol{\lambda}, M_z)), \qquad (1)$$

where we marginalized over a set of seven extrinsic parameters (distance, time, two sky position angles, and three Euler angles describing the source orientation) denoted with $\theta$. The probability $p(\theta)$ is a non-informative prior for these parameters. The likelihood is also maximized over the intrinsic property $M_z$ which then also serves as our reconstructed mass for the event.

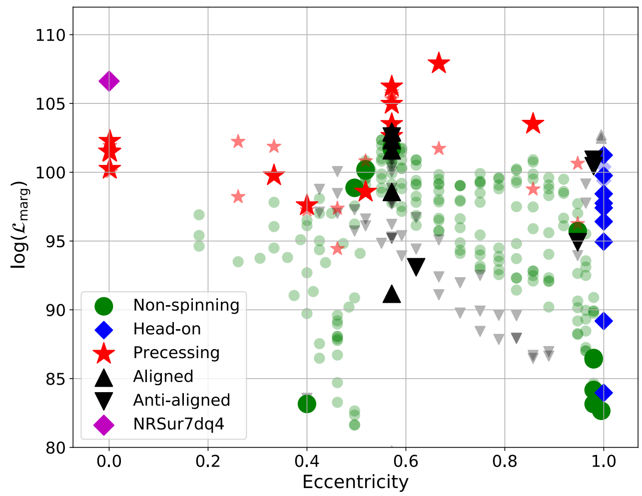


FIG. 1. **Marginalized likelihood as a function of eccentricity for our numerical relativity simulations explaining GW190521.** Each point corresponds to a separate numerical relativity simulation, categorized based on the black holes' spin (see legend). Categories include 'non-spinning' ($\chi_{\mathrm{eff}} = \chi_{\mathrm{P}} = 0$), 'head-on' ($e = 1$), 'precessing' ($\chi_{\mathrm{P}} > 0$), 'aligned' ($\chi_{\mathrm{eff}} > 0$) and 'anti-aligned' ($\chi_{\mathrm{eff}} < 0$). The simulations are further distinguished using a model-agnostic waveform consistency test. Large (small) marks correspond to simulations in which the reconstructed gravitational waveform is consistent (inconsistent) with the highest-likelihood waveform. We also include for comparison our likelihood estimate for the much more detailed set NRSur7dq4 of circular waveforms [50] used by LIGO/Virgo [3, 4] (purple) .

The marginal likelihood values from Eq. 1 for each numerical relativity simulation are shown in Fig. 1. We grouped waveforms with respect to the black holes' spin and spin orientation. While the parameter space is not evenly covered, we see that the obtained marginal likelihood values peak at $e \approx 0.7$ eccentricity and precession. In general, precessing waveforms correspond to higher marginal likelihoods than non-spinning or aligned/anti-aligned waveforms independently of eccentricity.

## IV. WAVEFORM CONSISTENCY TEST

Parameter estimation can determine the most likely gravitational-waveform. However, by itself it does not guarantee that the obtained waveform is indeed an accurate explanation of the observed data. This is particularly relevant for cases in which the parameter space explored in the estimation process does not cover the binary's true parameters, e.g. when eccentricity or precession are not properly accounted for.

We quantitatively tested the consistency between the observed gravitational wave signal and our numerical

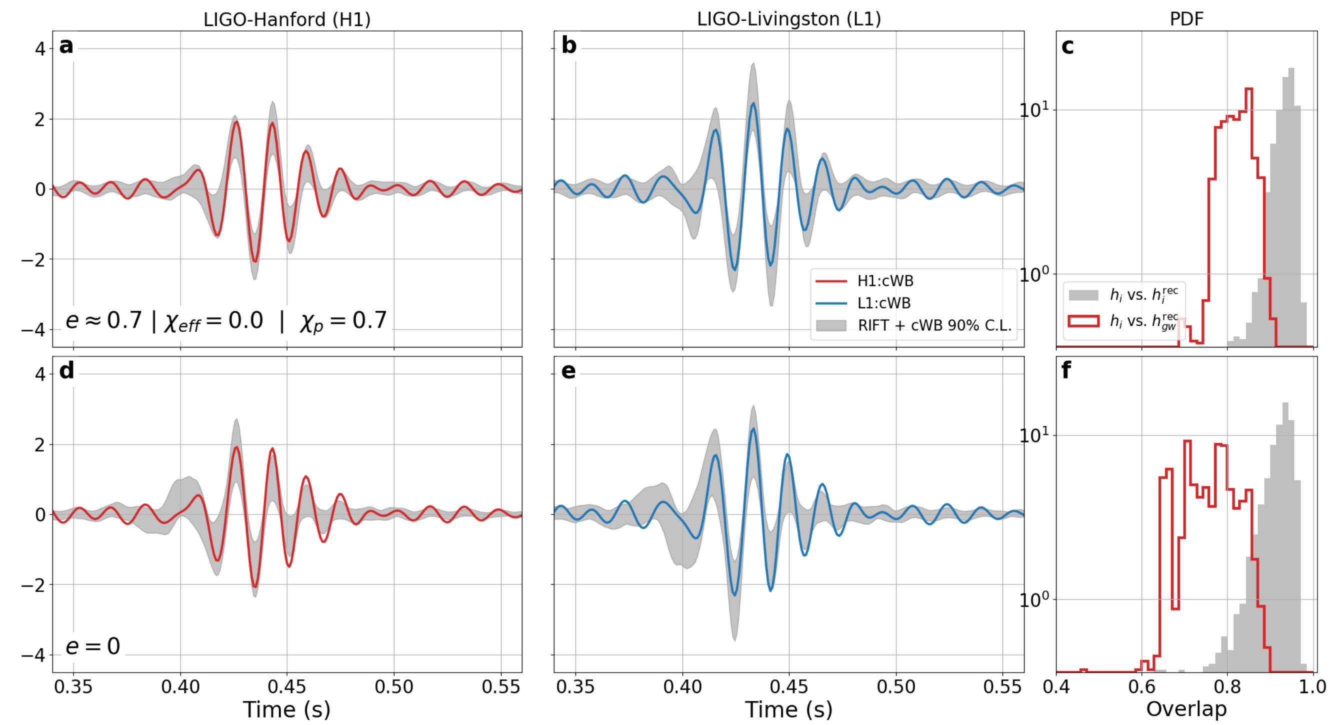


FIG. 2. **Consistency of the model-independent (cWB) reconstruction of GW190521 with the numerical relativity simulations**. Top panels - our high-eccentricity simulation, bottom panels - circular NRSur7dq4 simulations [50] for the LIGO-Hanford (a,d) and LIGO-Livingston (b,e) detectors. The colored lines in (a,b,d,e) show the cWB reconstruction of GW190521 (same as the cWB curve in Fig. 1 of [3]) together with the 90% confidence intervals calculated over the weighted RIFT samples injected into the off-source data and reconstructed with cWB. We see that the highly eccentric model (a,b) shows better waveform coherence with the cWB reconstruction (colored curves) than the circular NRSur7dq4 waveform model (d,e). The right column (c,f) shows the distributions of Overlap$(h_i, h_i^{\rm rec})$ and Overlap$(h_i, h_{gw}^{\rm rec})$ (see legend) demonstrating the agreement of both models with the cWB reconstruction.

relativity waveforms using a model-independent waveform reconstruction algorithm called coherent WaveBurst (cWB; [51–53]), which detected GW190521 with high significance [3]. This comparison provided a robust test of our numerical relativity waveforms in addition to the maximum likelihood statistic by RIFT.

For a given waveform $h_i$, we checked consistency with the recorded gravitational wave $h_{\rm gw}$ by using the following procedure [53]. We superimposed $h_i$ on the detector noise at the off-source time around the event and reconstructed both waveforms, denoted by $h_i^{\rm rec}$ and $h_{gw}^{\rm rec}$, using cWB. We quantified consistency between two waveforms $h_1$ and $h_2$ using a normalized+whitened cross-correlation we call "Overlap":

$$\mathrm{Overlap}(h_1, h_2) = \frac{(\hat{h}_1 \star \hat{h}_2)}{(\hat{h}_1 \star \hat{h}_1)(\hat{h}_2 \star \hat{h}_2)}\,. \tag{2}$$

Here, $\hat{h}_{\rm x}$ indicates spectral whitening of the waveform $h_{\rm x}$, which we applied in order to account for the detector noise spectrum. For a waveform that perfectly matches the incoming gravitational-wave signal, and in the presence of no noise, we would get Overlap$\,=1$.

For each numerical relativity waveform, we generated a weighted sample of $M_z, \boldsymbol{\lambda}$ and extrinsic parameters $\theta_k$ using RIFT, where weights were proportional to the likelihood of each set of parameters corresponding to observations. For a given parameter set $i$ we computed the corresponding gravitational waveform $h_{\rm i}$, and calculated Overlap$(h_{\rm i}, h_{gw}^{\rm rec})$. The distribution of Overlap$(h_{\rm i}, h_{gw}^{\rm rec})$ over the weighted samples for our highest-significance numerical-relativity simulation and the reference NRSur7dq4 simulation are shown in Fig. 2(c,f-black histograms).

The spread of the distribution of Overlap$(h_{\rm i}, h_{gw}^{\rm rec})$ is due to the uncertainty of the reconstructed binary parameters, the cWB waveform reconstruction and detector noise. To quantify the effect of the cWB waveform reconstruction and noise, we computed the off-source distribution of Overlap$(h_{\rm i}, h_i^{\rm rec})$ over our weighted samples, shown in Fig. 2(c,f-grey histograms), which is independent of the RIFT binary parameter estimation. Any significant separation of these two distributions would mean that the waveform model used by RIFT is inconsistent with the observations.

We characterized the separation between the two distributions by computing the probability $p_{\rm gw}$ that a randomly drawn value from the Overlap$(h_{\rm i}, h_{,gw}^{\rm rec})$ distribution is greater than a randomly drawn value from the

Overlap$(h_i, h^{\rm rec}_{,i})$ distribution. We considered those numerical relativity simulations consistent with the observations for which $p_{\rm gw} > 10^{-2}$. These are shown with large marks in Fig. 1. We see that only a minority of the numerical relativity simulations we carried out satisfy this criterion. Notably, the simulations with the highest $\log \mathcal{L}_{\rm marg}$ values for with $e > 0.6$ pass this criterion.

In Fig. 2 we show the gravitational waveform $\hat{h}^{\rm rec}_{gw}$ reconstructed by cWB and the 90% confidence intervals calculated over the weighted samples for our highest-significance numerical relativity simulation (a,b) and the reference NRSur7dq4 simulation (d,e). The confidence intervals are calculated from the waveforms $\hat{h}^{\rm rec}_{i}$ and take into account the model uncertainty of RIFT and the cWB reconstruction errors. Both models demonstrate agreement with the cWB reconstruction with a slight preference of the highly-eccentric model.

| Parameters | This work | LIGO/Virgo |
|---|---|---|
| Primary mass [$M_\odot$]. | $102^{+7}_{-11}$ | $85^{+21}_{-14}$ |
| Secondary mass [$M_\odot$] | $102^{+7}_{-11}$ | $66^{+17}_{-18}$ |
| Total mass [$M_\odot$] | $204^{+14}_{-33}$ | $150^{+29}_{-17}$ |
| Mass ratio | 1 | $0.79^{+0.19}_{-0.29}$ |
| Luminosity distance [Gpc] | $1.84^{+1.07}_{-0.054}$ | $5.3^{+2.4}_{-2.6}$ |
| Redshift | $0.35^{+0.16}_{-0.09}$ | $0.82^{+0.28}_{-0.34}$ |
| Eccentricity | 0.67 | 0 |
| Effective spin ($\chi_{\rm eff}$) | 0 | $0.08^{+0.27}_{-0.36}$ |
| Precession spin ($\chi_{\rm p}$) | 0.7 | $0.68^{+0.25}_{-0.37}$ |

TABLE I. **Reconstructed properties of GW190521** by this work. For comparison we also show the properties obtained by LIGO/Virgo [3, 4] using the NRSur7dq4 non-eccentric, precessing waveform model [50].

LIGO/Virgo carried out a binary parameter estimation for GW190521 and found evidence for precession [3]. The waveform family used for that analysis, however, did not include the possibility of eccentricity. A previous study showed that highly-eccentric, high-mass black hole mergers can be confused with precession if one uses a non-eccentric, precessing waveform model [20]. A separate study considered low-eccentricity, non-precessing waveforms and found that they match GW190521 observations similarly to precessing but non-eccentric waveforms [54, 55]. Our results support the presence of both precession and high eccentricity.

We list the binary parameters found by LIGO and those found by our analysis for the waveform with the highest $\log \mathcal{L}_{\rm marg}$ in Table I. We see that our reconstruction finds remarkably similar parameters than LIGO/Virgo, except for the eccentricity.

## V. ECCENTRICITY VS. NO ECCENTRICITY

We find a high-eccentricity model with $e \approx 0.7$ to have the highest likelihood, however our cWB consistency check also finds some of our $e = 0$ models to be consistent with observations. The difference in $\mathcal{L}_{\rm marg}$ between our highest likelihood model and the highest likelihood $e = 0$ model is $\Delta \log \mathcal{L}_{\rm marg} = 5.6$, corresponding to an effective Bayes factor of $\mathcal{B} \approx 300$. Taking into account that the zero-eccentricity case has one less estimated parameter through the Akaike information criterion, we find an effective Bayes factor of $\mathcal{B} \approx 100$.

We additionally computed $\mathcal{L}_{\rm marg}$ for the full NRSur7dq4 non-eccentric, precessing waveform model used by LIGO/Virgo [3, 4]. NRSur7dq4 is substantially more complete than our numerical relativity waveform family, in particular with respect to the binary's mass ratio, spin magnitude and spin direction. Despite this completeness, our $e \approx 0.7$ model has a higher $\mathcal{L}_{\rm marg}$ value than the NRSur7dq4 model. Although this difference is not substantial, with an effective Bayes factor of $\mathcal{B} \approx 4$ favoring the $e \approx 0.7$ model.

## VI. CONCLUSION

We carried out 325 numerical relativity simulations of black hole mergers to probe whether GW190521 could be an eccentric merger. These simulations are the first on this scale to include high eccentricity and spin-precession. Our comparison of these simulations to observed data shows that a high-eccentricity, precessing binary is the most consistent with the observed gravitational wave signal GW190521 than the precessing but circular waveform identified by LIGO/Virgo.

Within our limited sampling of the mass ratio and the spin parameter space, high eccentricity is favored over $e = 0$ with an effective Bayes factor of $\mathcal{B} = 100$. However, compared to a the densely sampled NRSur7dq4 waveform model, high eccentricity is favored with $\mathcal{B} = 4$. Further simulations will help to determine the effect of limited sampling and could provide further supporting evidence of high-eccentricity for GW190521.

Eccentricity in GW190521 points to the same direction as its other properties. The origin of this merger is most consistent with a hierarchical black hole merger as a consequence of chance encounters. High black hole spin is expected if the black hole is forged in the merger of smaller black holes. Gravitational capture in a chance encounter is expected to bring together two black holes with randomly oriented spins, with the black hole spins typically misaligned from the binary orbit, resulting in high $\chi_{\rm p}$. Such misaligned spins are not expected if the binary is a remnant of a stellar binary system. Chance encounters naturally lead to eccentric binary orbits, while no eccentricity is expected for a stellar binary origin. Finally, the masses of the black holes are $> 65\,{\rm M}_\odot$ and are therefore too high to be explained by stellar evolution.

A hierarchical merger origin naturally explains such high masses without invoking new physics.


## ACKNOWLEDGMENTS

The authors would like to thank Erik Katsavounidis for useful suggestions, and Gabriele Vedovato for his valuable help with the cWB search algorithm and with the setup of the cWB waveform consistency study. The authors gratefully acknowledge the National Science Foundation (NSF) for financial support from Grants No. PHY-1912632, No. PHY-1806165, No. PHY-1707946, No. ACI-1550436, No. AST-1516150, No. ACI-1516125, No. PHY-1726215, and the support of the Alfred P. Sloan Foundation. This work used the Extreme Science and Engineering Discovery Environment (XSEDE) [allocation TG-PHY060027N], which is supported by NSF grant No. ACI-1548562 and Frontera projects PHY-20010 and PHY-20007. Computational resources were also provided by the NewHorizons, BlueSky Clusters, and Green Prairies at the Rochester Institute of Technology, which were supported by NSF grants No. PHY-0722703, No. DMS-0820923, No. AST-1028087, No. PHY-1229173, and No. PHY-1726215.



[1] J. Aasi *et al.*, Class. Quantum Grav. **32**, 074001 (2015).
[2] F. Acernese *et al.*, Class. Quantum Grav. **32**, 024001 (2015).
[3] R. Abbott *et al.*, Phys. Rev. Lett. **125**, 101102 (2020).
[4] R. Abbott *et al.*, Astrophys. J. **900**, L13 (2020).
[5] D. Gerosa and E. Berti, Phys. Rev. D **95**, 124046 (2017).
[6] M. Fishbach, D. E. Holz, and B. Farr, Astrophys. J. Lett. **840**, L24 (2017).
[7] Y. Yang *et al.*, Phys. Rev. Lett. **123**, 181101 (2019).
[8] I. Mandel and R. O'Shaughnessy, Class. Quantum Grav. **27**, 114007 (2010).
[9] K. Breivik *et al.*, Astrophys. J. Lett. **830**, L18 (2016).
[10] J. Samsing, Phys. Rev. D **97**, 103014 (2018).
[11] C. L. Rodriguez *et al.*, Phys. Rev. D **98**, 123005 (2018).
[12] R. M. O'Leary, B. Kocsis, and A. Loeb, Mon. Notices Royal Astron. Soc **395**, 2127 (2009).
[13] G. Fragione, E. Grishin, N. W. C. Leigh, H. B. Perets, and R. Perna, Mon. Notices Royal Astron. Soc **488**, 47 (2019).
[14] C. L. Rodriguez and F. Antonini, Astrophys. J. **863**, 7 (2018).
[15] F. Antonini *et al.*, Astrophys. J. **816**, 65 (2016), arXiv:1509.05080.
[16] F. Antonini and F. A. Rasio, Astrophys. J. **831**, 187 (2016).
[17] F. Antonini and H. B. Perets, Astrophys. J. **757**, 27 (2012).
[18] A. Ramos-Buades, S. Tiwari, M. Haney, and S. Husa, Phys. Rev. D **102**, 043005 (2020).
[19] B. P. Abbott *et al.*, Astrophys. J. **883**, 149 (2019).
[20] J. C. Bustillo, N. Sanchis-Gual, A. Torres-Forné, and J. A. Font, arXiv:2009.01066 (2020).
[21] I. M. Romero-Shaw, P. D. Lasky, and E. Thrane, Mon. Notices Royal Astron. Soc **490**, 5210 (2019).
[22] W. E. East, S. T. McWilliams, J. Levin, and F. Pretorius, Phys. Rev. D **87**, 043004 (2013).
[23] A. Ramos-Buades *et al.*, Phys. Rev. D **101**, 083015 (2020).
[24] B. Ireland, O. Birnholtz, H. Nakano, E. West, and M. Campanelli, Phys. Rev. D **100**, 024015 (2019).
[25] J. Lange, R. O'Shaughnessy, and M. Rizzo, arXiv:1805.10457 (2018).
[26] J. Lange *et al.*, Phys. Rev. D **96**, 104041 (2017).
[27] B. P. Abbott *et al.*, Phys. Rev. D **94**, 064035 (2016).
[28] J. Healy *et al.*, Phys. Rev. D **97**, 064027 (2018).
[29] Y. Zlochower, J. G. Baker, M. Campanelli, and C. O. Lousto, Phys. Rev. D **72**, 024021 (2005).
[30] M. Campanelli, C. O. Lousto, P. Marronetti, and Y. Zlochower, Phys. Rev. Lett. **96**, 111101 (2006).
[31] T. Nakamura, K. Oohara, and Y. Kojima, Prog. Theor. Phys. Suppl. **90**, 1 (1987).
[32] M. Shibata and T. Nakamura, Phys. Rev. **D52**, 5428 (1995).
[33] T. W. Baumgarte and S. L. Shapiro, Phys. Rev. **D59**, 024007 (1998).
[34] C. O. Lousto and Y. Zlochower, Phys. Rev. **D77**, 024034 (2008).
[35] Y. Zlochower, M. Ponce, and C. O. Lousto, Phys. Rev. **D86**, 104056 (2012).
[36] J. Healy and C. O. Lousto, Phys. Rev. D **95**, 024037 (2017).
[37] J. Healy, C. O. Lousto, Y. Zlochower, and M. Campanelli, Class. Quant. Grav. **34**, 224001 (2017).
[38] J. Healy *et al.*, Phys. Rev. D **100**, 024021 (2019).
[39] J. Healy and C. O. Lousto, arXiv:2007.07910 (2020).
[40] F. Löffler *et al.*, Class. Quant. Grav. **29**, 115001 (2012).
[41] `http://einsteintoolkit.org`.
[42] `http://cactuscode.org`.
[43] E. Schnetter, S. H. Hawley, and I. Hawke, Class. Quant. Grav. **21**, 1465 (2004).
[44] S. Brandt and B. Brügmann, Phys. Rev. Lett. **78**, 3606 (1997).
[45] M. Ansorg, B. Brügmann, and W. Tichy, Phys. Rev. **D70**, 064011 (2004).
[46] J. Healy, C. O. Lousto, H. Nakano, and Y. Zlochower, Class. Quant. Grav. **34**, 145011 (2017).
[47] H. Nakano, J. Healy, C. O. Lousto, and Y. Zlochower, Phys. Rev. **D91**, 104022 (2015).
[48] M. Campanelli, C. O. Lousto, H. Nakano, and Y. Zlochower, Phys. Rev. **D79**, 084010 (2009).
[49] C. Reisswig and D. Pollney, Class. Quant. Grav. **28**, 195015 (2011).
[50] V. Varma *et al.*, Phys. Rev. Research **1**, 033015 (2019).
[51] S. Klimenko, S. Mohanty, M. Rakhmanov, and G. Mitselmakher, Phys. Rev. D **72**, 122002 (2005).
[52] S. Klimenko *et al.*, Phys. Rev. **D93**, 042004 (2016).
[53] F. Salemi *et al.*, Phys. Rev. D **100**, 042003 (2019).
[54] I. Romero-Shaw *et al.*, GW190521: orbital eccentricity and signatures of dynamical formation in a binary black hole merger signal, (in Prep).

[55] M. E. Lower, E. Thrane, P. D. Lasky, and R. Smith, Physical Review D **98** (2018).

## A. SUPPLEMENTARY MATERIAL

| No | $m_1$ $[M_\odot]$ | $m_2$ $[M_\odot]$ | $M$ $[M_\odot]$ | q | D $[Gpc]$ | z | e | $\chi_{eff}$ | $\chi_p$ | $\log \mathcal{L}_{\rm marg}$ | Consistency |
|---|---|---|---|---|---|---|---|---|---|---|---|
| **Non-spinning eBBH runs** | | | | | | | | | | | |
| 1 | $113^{+16}_{-20}$ | $16^{+2}_{-3}$ | $129^{+19}_{-23}$ | 0.14 | $2.14^{+0.54}_{-0.47}$ | $0.39^{+0.08}_{-0.08}$ | 0.46 | 0.0 | 0.0 | 84.71 | N |
| 2 | $128^{+5}_{-9}$ | $18^{+1}_{-1}$ | $146^{+6}_{-10}$ | 0.14 | $1.97^{+0.38}_{-0.33}$ | $0.37^{+0.06}_{-0.05}$ | 0.5 | 0.0 | 0.0 | 98.77 | N |
| 3 | $137^{+4}_{-8}$ | $20^{+1}_{-1}$ | $156^{+5}_{-9}$ | 0.14 | $1.64^{+0.26}_{-0.16}$ | $0.31^{+0.04}_{-0.03}$ | 0.52 | 0.0 | 0.0 | 99.09 | N |
| 4 | $144^{+3}_{-6}$ | $21^{+0}_{-1}$ | $164^{+4}_{-7}$ | 0.14 | $1.27^{+0.22}_{-0.21}$ | $0.25^{+0.04}_{-0.04}$ | 0.55 | 0.0 | 0.0 | 98.85 | N |
| 5 | $149^{+0}_{-9}$ | $21^{+0}_{-1}$ | $170^{+0}_{-10}$ | 0.14 | $1.17^{+0.2}_{-0.04}$ | $0.23^{+0.03}_{-0.01}$ | 0.57 | 0.0 | 0.0 | 97.77 | N |
| 6 | $145^{+8}_{-5}$ | $21^{+1}_{-1}$ | $166^{+9}_{-6}$ | 0.14 | $1.16^{+0.19}_{-0.19}$ | $0.23^{+0.03}_{-0.03}$ | 0.59 | 0.0 | 0.0 | 97.16 | N |
| 7 | $150^{+7}_{-7}$ | $21^{+1}_{-1}$ | $171^{+8}_{-8}$ | 0.14 | $0.95^{+0.16}_{-0.27}$ | $0.2^{+0.03}_{-0.05}$ | 0.62 | 0.0 | 0.0 | 96.14 | N |
| 8 | $158^{+0}_{-7}$ | $23^{+0}_{-1}$ | $181^{+0}_{-8}$ | 0.14 | $0.78^{+0.13}_{-0.01}$ | $0.16^{+0.02}_{-0.0}$ | 0.67 | 0.0 | 0.0 | 95.76 | N |
| 9 | $153^{+7}_{-5}$ | $22^{+1}_{-1}$ | $174^{+8}_{-5}$ | 0.14 | $0.7^{+0.12}_{-0.12}$ | $0.15^{+0.02}_{-0.02}$ | 0.71 | 0.0 | 0.0 | 94.1 | N |
| 10 | $154^{+9}_{-5}$ | $22^{+1}_{-1}$ | $176^{+10}_{-6}$ | 0.14 | $0.52^{+0.18}_{-0.1}$ | $0.11^{+0.04}_{-0.02}$ | 0.75 | 0.0 | 0.0 | 93.19 | N |
| 11 | $156^{+6}_{-6}$ | $22^{+1}_{-1}$ | $178^{+7}_{-7}$ | 0.14 | $0.44^{+0.14}_{-0.09}$ | $0.1^{+0.03}_{-0.02}$ | 0.79 | 0.0 | 0.0 | 92.56 | N |
| 12 | $160^{+0}_{-12}$ | $23^{+0}_{-2}$ | $182^{+0}_{-14}$ | 0.14 | $0.45^{+0.0}_{-0.09}$ | $0.1^{+0.0}_{-0.02}$ | 0.82 | 0.0 | 0.0 | 91.44 | N |
| 13 | $156^{+6}_{-5}$ | $22^{+1}_{-1}$ | $178^{+7}_{-6}$ | 0.14 | $0.3^{+0.09}_{-0.1}$ | $0.07^{+0.02}_{-0.02}$ | 0.86 | 0.0 | 0.0 | 92.09 | N |
| 14 | $157^{+6}_{-12}$ | $22^{+1}_{-2}$ | $180^{+7}_{-14}$ | 0.14 | $0.25^{+0.06}_{-0.1}$ | $0.06^{+0.01}_{-0.02}$ | 0.89 | 0.0 | 0.0 | 90.2 | N |
| 15 | $166^{+3}_{-10}$ | $24^{+0}_{-1}$ | $190^{+4}_{-11}$ | 0.14 | $0.14^{+0.02}_{-0.04}$ | $0.03^{+0.0}_{-0.01}$ | 0.95 | 0.0 | 0.0 | 88.22 | N |
| 16 | $163^{+5}_{-5}$ | $23^{+1}_{-1}$ | $186^{+5}_{-6}$ | 0.14 | $0.1^{+0.02}_{-0.03}$ | $0.02^{+0.0}_{-0.01}$ | 0.96 | 0.0 | 0.0 | 87.26 | N |
| 17 | $154^{+14}_{-4}$ | $22^{+2}_{-1}$ | $177^{+16}_{-5}$ | 0.14 | $0.28^{+0.08}_{-0.21}$ | $0.06^{+0.02}_{-0.05}$ | 0.98 | 0.0 | 0.0 | 84.17 | Y |
| 18 | $156^{+11}_{-8}$ | $22^{+2}_{-1}$ | $178^{+13}_{-9}$ | 0.14 | $0.33^{+0.08}_{-0.09}$ | $0.07^{+0.02}_{-0.02}$ | 0.99 | 0.0 | 0.0 | 77.62 | N |
| 19 | $131^{+4}_{-8}$ | $22^{+1}_{-1}$ | $153^{+5}_{-10}$ | 0.17 | $2.33^{+0.17}_{-0.39}$ | $0.42^{+0.03}_{-0.06}$ | 0.4 | −0.0 | 0.0 | 83.16 | Y |
| 20 | $127^{+0}_{-29}$ | $21^{+0}_{-5}$ | $148^{+0}_{-33}$ | 0.17 | $1.85^{+0.55}_{-0.02}$ | $0.35^{+0.09}_{-0.0}$ | 0.43 | −0.0 | 0.0 | 86.48 | N |
| 21 | $117^{+7}_{-19}$ | $20^{+1}_{-3}$ | $137^{+8}_{-22}$ | 0.17 | $2.36^{+0.4}_{-0.36}$ | $0.43^{+0.06}_{-0.06}$ | 0.46 | −0.0 | 0.0 | 87.77 | N |
| 22 | $122^{+8}_{-5}$ | $20^{+1}_{-1}$ | $143^{+9}_{-6}$ | 0.17 | $2.28^{+0.3}_{-0.42}$ | $0.42^{+0.05}_{-0.07}$ | 0.5 | −0.0 | 0.0 | 98.87 | Y |
| 23 | $132^{+8}_{-5}$ | $22^{+1}_{-1}$ | $154^{+10}_{-6}$ | 0.17 | $1.91^{+0.25}_{-0.28}$ | $0.36^{+0.04}_{-0.05}$ | 0.52 | −0.0 | 0.0 | 99.57 | N |
| 24 | $137^{+5}_{-5}$ | $23^{+1}_{-1}$ | $160^{+6}_{-5}$ | 0.17 | $1.52^{+0.36}_{-0.09}$ | $0.3^{+0.06}_{-0.02}$ | 0.55 | −0.0 | 0.0 | 98.54 | N |
| 25 | $138^{+4}_{-7}$ | $23^{+1}_{-1}$ | $161^{+5}_{-8}$ | 0.17 | $1.53^{+0.26}_{-0.29}$ | $0.3^{+0.04}_{-0.05}$ | 0.57 | −0.0 | 0.0 | 98.71 | N |
| 26 | $143^{+7}_{-5}$ | $24^{+1}_{-1}$ | $167^{+8}_{-6}$ | 0.17 | $1.24^{+0.23}_{-0.14}$ | $0.25^{+0.04}_{-0.02}$ | 0.59 | −0.0 | 0.0 | 97.5 | N |
| 27 | $144^{+7}_{-4}$ | $24^{+1}_{-1}$ | $168^{+9}_{-4}$ | 0.17 | $1.11^{+0.22}_{-0.13}$ | $0.22^{+0.04}_{-0.02}$ | 0.62 | −0.0 | 0.0 | 96.86 | N |
| 28 | $146^{+6}_{-9}$ | $24^{+1}_{-2}$ | $171^{+7}_{-11}$ | 0.17 | $0.96^{+0.16}_{-0.23}$ | $0.2^{+0.03}_{-0.04}$ | 0.67 | −0.0 | 0.0 | 95.71 | N |
| 29 | $149^{+6}_{-6}$ | $25^{+1}_{-1}$ | $174^{+7}_{-8}$ | 0.17 | $0.81^{+0.16}_{-0.16}$ | $0.17^{+0.03}_{-0.03}$ | 0.71 | −0.0 | 0.0 | 94.34 | N |
| 30 | $150^{+5}_{-5}$ | $25^{+1}_{-1}$ | $175^{+6}_{-5}$ | 0.17 | $0.69^{+0.13}_{-0.1}$ | $0.15^{+0.02}_{-0.02}$ | 0.75 | −0.0 | 0.0 | 92.98 | N |
| 31 | $152^{+6}_{-6}$ | $25^{+1}_{-1}$ | $177^{+7}_{-7}$ | 0.17 | $0.53^{+0.13}_{-0.11}$ | $0.11^{+0.03}_{-0.02}$ | 0.79 | −0.0 | 0.0 | 92.91 | N |
| 32 | $152^{+6}_{-8}$ | $25^{+1}_{-1}$ | $177^{+6}_{-10}$ | 0.17 | $0.43^{+0.11}_{-0.16}$ | $0.09^{+0.02}_{-0.03}$ | 0.82 | −0.0 | 0.0 | 92.32 | N |
| 33 | $154^{+5}_{-7}$ | $26^{+1}_{-1}$ | $180^{+6}_{-8}$ | 0.17 | $0.34^{+0.13}_{-0.1}$ | $0.07^{+0.03}_{-0.02}$ | 0.86 | 0.0 | 0.0 | 92.49 | N |
| 34 | $155^{+5}_{-9}$ | $26^{+1}_{-1}$ | $181^{+6}_{-10}$ | 0.17 | $0.26^{+0.11}_{-0.08}$ | $0.06^{+0.02}_{-0.02}$ | 0.89 | 0.0 | 0.0 | 92.06 | N |
| 35 | $158^{+5}_{-10}$ | $26^{+1}_{-2}$ | $184^{+6}_{-12}$ | 0.17 | $0.14^{+0.05}_{-0.05}$ | $0.03^{+0.01}_{-0.01}$ | 0.95 | −0.0 | 0.0 | 89.19 | N |
| 36 | $159^{+9}_{-4}$ | $26^{+1}_{-1}$ | $185^{+10}_{-5}$ | 0.17 | $0.12^{+0.03}_{-0.03}$ | $0.03^{+0.01}_{-0.01}$ | 0.96 | −0.0 | 0.0 | 87.02 | N |
| 37 | $152^{+11}_{-10}$ | $25^{+2}_{-2}$ | $177^{+13}_{-12}$ | 0.17 | $0.34^{+0.07}_{-0.26}$ | $0.07^{+0.01}_{-0.06}$ | 0.98 | 0.0 | 0.0 | 83.59 | N |
| 38 | $150^{+10}_{-13}$ | $25^{+2}_{-2}$ | $175^{+11}_{-15}$ | 0.17 | $0.36^{+0.07}_{-0.11}$ | $0.08^{+0.01}_{-0.02}$ | 0.99 | 0.0 | 0.0 | 77.25 | Y |
| 39 | $124^{+6}_{-5}$ | $25^{+1}_{-1}$ | $149^{+7}_{-7}$ | 0.2 | $2.33^{+0.39}_{-0.4}$ | $0.42^{+0.06}_{-0.06}$ | 0.43 | −0.0 | 0.0 | 94.37 | N |
| 40 | $114^{+8}_{-28}$ | $23^{+2}_{-6}$ | $137^{+9}_{-33}$ | 0.2 | $2.42^{+0.69}_{-0.07}$ | $0.44^{+0.1}_{-0.01}$ | 0.46 | −0.0 | 0.0 | 83.28 | N |
| 41 | $120^{+6}_{-7}$ | $24^{+1}_{-1}$ | $145^{+7}_{-9}$ | 0.2 | $2.62^{+0.36}_{-0.36}$ | $0.47^{+0.05}_{-0.05}$ | 0.5 | −0.0 | 0.0 | 98.9 | N |
| 42 | $125^{+10}_{-6}$ | $25^{+2}_{-1}$ | $150^{+12}_{-7}$ | 0.2 | $2.4^{+0.15}_{-0.67}$ | $0.44^{+0.02}_{-0.1}$ | 0.52 | −0.0 | 0.0 | 99.52 | N |
| 43 | $132^{+6}_{-5}$ | $26^{+1}_{-1}$ | $158^{+7}_{-6}$ | 0.2 | $1.92^{+0.2}_{-0.31}$ | $0.36^{+0.03}_{-0.05}$ | 0.55 | −0.0 | 0.0 | 99.54 | N |
| 44 | $134^{+8}_{-4}$ | $27^{+2}_{-1}$ | $161^{+9}_{-5}$ | 0.2 | $1.82^{+0.19}_{-0.31}$ | $0.34^{+0.03}_{-0.05}$ | 0.57 | −0.0 | 0.0 | 99.15 | N |
| 45 | $136^{+6}_{-5}$ | $27^{+1}_{-1}$ | $163^{+8}_{-6}$ | 0.2 | $1.65^{+0.12}_{-0.51}$ | $0.32^{+0.02}_{-0.09}$ | 0.59 | −0.0 | 0.0 | 98.81 | N |
| 46 | $141^{+8}_{-6}$ | $28^{+2}_{-1}$ | $169^{+9}_{-7}$ | 0.2 | $1.4^{+0.32}_{-0.23}$ | $0.27^{+0.05}_{-0.04}$ | 0.62 | −0.0 | 0.0 | 97.82 | N |
| 47 | $142^{+6}_{-5}$ | $28^{+1}_{-1}$ | $170^{+7}_{-6}$ | 0.2 | $1.17^{+0.09}_{-0.26}$ | $0.23^{+0.02}_{-0.05}$ | 0.67 | −0.0 | 0.0 | 96.5 | N |
| 48 | $143^{+7}_{-4}$ | $29^{+1}_{-1}$ | $172^{+9}_{-5}$ | 0.2 | $0.97^{+0.18}_{-0.22}$ | $0.2^{+0.03}_{-0.04}$ | 0.71 | 0.0 | 0.0 | 94.87 | N |
| 49 | $144^{+7}_{-5}$ | $29^{+1}_{-1}$ | $173^{+9}_{-6}$ | 0.2 | $0.81^{+0.13}_{-0.22}$ | $0.17^{+0.02}_{-0.04}$ | 0.75 | −0.0 | 0.0 | 94.34 | N |
| 50 | $148^{+4}_{-7}$ | $30^{+1}_{-1}$ | $178^{+5}_{-9}$ | 0.2 | $0.57^{+0.16}_{-0.27}$ | $0.12^{+0.03}_{-0.05}$ | 0.79 | 0.0 | 0.0 | 93.88 | N |
| 51 | $149^{+7}_{-6}$ | $30^{+1}_{-1}$ | $178^{+9}_{-8}$ | 0.2 | $0.48^{+0.16}_{-0.17}$ | $0.1^{+0.03}_{-0.03}$ | 0.82 | 0.0 | 0.0 | 92.31 | N |
| 52 | $149^{+8}_{-8}$ | $30^{+2}_{-2}$ | $179^{+9}_{-10}$ | 0.2 | $0.39^{+0.15}_{-0.13}$ | $0.09^{+0.03}_{-0.03}$ | 0.86 | 0.0 | 0.0 | 92.82 | N |
| 53 | $150^{+9}_{-5}$ | $30^{+2}_{-1}$ | $180^{+10}_{-6}$ | 0.2 | $0.31^{+0.16}_{-0.1}$ | $0.07^{+0.03}_{-0.02}$ | 0.89 | 0.0 | 0.0 | 92.1 | N |

| | | | | | | | | | | | |
|---|---|---|---|---|---|---|---|---|---|---|---|
| 54 | $152^{+7}_{-6}$ | $30^{+1}_{-1}$ | $183^{+8}_{-7}$ | 0.2 | $0.17^{+0.07}_{-0.05}$ | $0.04^{+0.01}_{-0.01}$ | 0.95 | 0.0 | 0.0 | 88.27 | N |
| 55 | $158^{+4}_{-16}$ | $32^{+1}_{-3}$ | $190^{+4}_{-20}$ | 0.2 | $0.12^{+0.11}_{-0.01}$ | $0.03^{+0.02}_{-0.0}$ | 0.96 | 0.0 | 0.0 | 88.46 | N |
| 56 | $148^{+15}_{-11}$ | $30^{+3}_{-2}$ | $178^{+18}_{-13}$ | 0.2 | $0.37^{+0.1}_{-0.29}$ | $0.08^{+0.03}_{-0.05}$ | 0.98 | 0.0 | 0.0 | 83.15 | Y |
| 57 | $146^{+7}_{-17}$ | $29^{+1}_{-3}$ | $175^{+9}_{-21}$ | 0.2 | $0.4^{+0.1}_{-0.13}$ | $0.09^{+0.02}_{-0.03}$ | 0.99 | 0.0 | 0.0 | 78.22 | N |
| 58 | $109^{+15}_{-4}$ | $27^{+4}_{-1}$ | $136^{+19}_{-5}$ | 0.25 | $3.14^{+0.41}_{-0.62}$ | $0.54^{+0.06}_{-0.09}$ | 0.4 | 0.0 | 0.0 | 92.69 | N |
| 59 | $113^{+17}_{-8}$ | $28^{+4}_{-2}$ | $141^{+21}_{-10}$ | 0.25 | $3.0^{+0.5}_{-1.08}$ | $0.52^{+0.07}_{-0.16}$ | 0.43 | 0.0 | 0.0 | 87.54 | N |
| 60 | $109^{+6}_{-9}$ | $27^{+1}_{-2}$ | $136^{+7}_{-12}$ | 0.25 | $3.12^{+0.81}_{-0.33}$ | $0.54^{+0.11}_{-0.05}$ | 0.46 | 0.0 | 0.0 | 86.71 | N |
| 61 | $108^{+9}_{0}$ | $27^{+2}_{0}$ | $134^{+11}_{0}$ | 0.25 | $3.53^{+0.0}_{-0.82}$ | $0.6^{+0.0}_{-0.12}$ | 0.5 | −0.0 | 0.0 | 97.55 | N |
| 62 | $115^{+10}_{-2}$ | $29^{+2}_{-1}$ | $144^{+12}_{-3}$ | 0.25 | $3.12^{+0.19}_{-0.6}$ | $0.54^{+0.03}_{-0.09}$ | 0.52 | 0.0 | 0.0 | 100.12 | Y |
| 63 | $124^{+5}_{-10}$ | $31^{+1}_{-3}$ | $155^{+6}_{-13}$ | 0.25 | $2.46^{+0.44}_{-0.38}$ | $0.44^{+0.07}_{-0.06}$ | 0.55 | 0.0 | 0.0 | 99.87 | N |
| 64 | $127^{+8}_{-6}$ | $32^{+2}_{-2}$ | $159^{+10}_{-8}$ | 0.25 | $2.2^{+0.37}_{-0.35}$ | $0.4^{+0.06}_{-0.05}$ | 0.57 | 0.0 | 0.0 | 99.92 | N |
| 65 | $130^{+7}_{-7}$ | $33^{+2}_{-2}$ | $163^{+9}_{-8}$ | 0.25 | $1.96^{+0.38}_{-0.44}$ | $0.37^{+0.07}_{-0.06}$ | 0.59 | 0.0 | 0.0 | 99.19 | N |
| 66 | $135^{+0}_{-4}$ | $34^{+0}_{-1}$ | $169^{+0}_{-5}$ | 0.25 | $1.73^{+0.0}_{-0.14}$ | $0.33^{+0.0}_{-0.02}$ | 0.62 | 0.0 | 0.0 | 98.25 | N |
| 67 | $139^{+5}_{-7}$ | $35^{+1}_{-2}$ | $174^{+6}_{-9}$ | 0.25 | $1.28^{+0.38}_{-0.17}$ | $0.25^{+0.06}_{-0.03}$ | 0.67 | 0.0 | 0.0 | 96.65 | N |
| 68 | $138^{+7}_{-4}$ | $35^{+2}_{-1}$ | $173^{+8}_{-5}$ | 0.25 | $1.21^{+0.16}_{-0.23}$ | $0.24^{+0.03}_{-0.04}$ | 0.71 | −0.0 | 0.0 | 95.97 | N |
| 69 | $137^{+4}_{-1}$ | $34^{+1}_{0}$ | $171^{+5}_{-1}$ | 0.25 | $0.81^{+0.21}_{0.0}$ | $0.17^{+0.04}_{0.0}$ | 0.75 | −0.0 | 0.0 | 93.99 | N |
| 70 | $142^{+7}_{-5}$ | $36^{+2}_{-1}$ | $178^{+9}_{-7}$ | 0.25 | $0.65^{+0.24}_{-0.35}$ | $0.14^{+0.04}_{-0.07}$ | 0.79 | 0.0 | 0.0 | 93.53 | N |
| 71 | $137^{+7}_{0}$ | $34^{+2}_{0}$ | $171^{+9}_{0}$ | 0.25 | $0.65^{+0.07}_{-0.14}$ | $0.14^{+0.01}_{-0.03}$ | 0.82 | 0.0 | 0.0 | 93.73 | N |
| 72 | $144^{+4}_{-8}$ | $36^{+1}_{-2}$ | $180^{+5}_{-9}$ | 0.25 | $0.46^{+0.13}_{-0.15}$ | $0.1^{+0.03}_{-0.03}$ | 0.86 | 0.0 | 0.0 | 92.81 | N |
| 73 | $142^{+0}_{0}$ | $35^{+0}_{0}$ | $177^{+0}_{0}$ | 0.25 | $0.32^{+0.0}_{0.0}$ | $0.07^{+0.0}_{0.0}$ | 0.89 | 0.0 | 0.0 | 92.33 | N |
| 74 | $148^{+6}_{-6}$ | $37^{+1}_{-1}$ | $185^{+7}_{-7}$ | 0.25 | $0.2^{+0.06}_{-0.08}$ | $0.05^{+0.01}_{-0.02}$ | 0.95 | 0.0 | 0.0 | 90.64 | N |
| 75 | $140^{+7}_{0}$ | $35^{+2}_{0}$ | $175^{+9}_{0}$ | 0.25 | $0.13^{+0.05}_{0.0}$ | $0.03^{+0.01}_{0.0}$ | 0.96 | 0.0 | 0.0 | 87.0 | N |
| 76 | $139^{+17}_{-8}$ | $35^{+4}_{-2}$ | $174^{+22}_{-10}$ | 0.25 | $0.43^{+0.1}_{-0.34}$ | $0.09^{+0.02}_{-0.07}$ | 0.98 | 0.0 | 0.0 | 84.66 | N |
| 77 | $138^{+10}_{-9}$ | $35^{+2}_{-2}$ | $173^{+12}_{-12}$ | 0.25 | $0.49^{+0.11}_{-0.14}$ | $0.11^{+0.02}_{-0.03}$ | 0.99 | 0.0 | 0.0 | 78.13 | Y |
| 78 | $110^{+7}_{-6}$ | $37^{+2}_{-2}$ | $147^{+10}_{-8}$ | 0.33 | $3.3^{+0.47}_{-0.57}$ | $0.57^{+0.07}_{-0.08}$ | 0.18 | 0.0 | 0.0 | 95.4 | N |
| 79 | $112^{+4}_{-9}$ | $37^{+1}_{-3}$ | $149^{+6}_{-12}$ | 0.33 | $3.05^{+0.66}_{-0.46}$ | $0.53^{+0.09}_{-0.07}$ | 0.33 | −0.0 | 0.0 | 96.05 | N |
| 80 | $111^{+6}_{-8}$ | $37^{+2}_{-3}$ | $147^{+8}_{-11}$ | 0.33 | $3.33^{+0.62}_{-0.75}$ | $0.57^{+0.1}_{-0.09}$ | 0.4 | 0.0 | 0.0 | 89.73 | N |
| 81 | $114^{+0}_{-10}$ | $38^{+0}_{-3}$ | $152^{+1}_{-13}$ | 0.33 | $2.91^{+0.92}_{0.0}$ | $0.51^{+0.13}_{0.0}$ | 0.43 | 0.0 | 0.0 | 97.0 | N |
| 82 | $99^{+10}_{-3}$ | $33^{+3}_{-1}$ | $132^{+13}_{-4}$ | 0.33 | $3.22^{+1.1}_{-0.03}$ | $0.56^{+0.15}_{-0.0}$ | 0.46 | −0.0 | 0.0 | 88.06 | N |
| 83 | $101^{+8}_{-6}$ | $34^{+3}_{-2}$ | $135^{+10}_{-8}$ | 0.33 | $4.01^{+0.87}_{-0.57}$ | $0.67^{+0.12}_{-0.08}$ | 0.5 | 0.0 | 0.0 | 96.24 | N |
| 84 | $112^{+2}_{-8}$ | $37^{+1}_{-3}$ | $149^{+2}_{-10}$ | 0.33 | $3.37^{+0.85}_{-0.11}$ | $0.58^{+0.12}_{-0.02}$ | 0.52 | 0.0 | 0.0 | 100.22 | Y |
| 85 | $116^{+2}_{-5}$ | $39^{+1}_{-2}$ | $155^{+3}_{-7}$ | 0.33 | $2.75^{+0.81}_{-0.0}$ | $0.49^{+0.12}_{-0.0}$ | 0.55 | 0.0 | 0.0 | 100.81 | N |
| 86 | $117^{+6}_{-3}$ | $39^{+2}_{-1}$ | $156^{+8}_{-5}$ | 0.33 | $2.96^{+0.16}_{-0.61}$ | $0.52^{+0.02}_{-0.09}$ | 0.57 | −0.0 | 0.0 | 100.66 | N |
| 87 | $120^{+7}_{-7}$ | $40^{+2}_{-2}$ | $160^{+9}_{-10}$ | 0.33 | $2.55^{+0.34}_{-0.69}$ | $0.46^{+0.05}_{-0.11}$ | 0.59 | 0.0 | 0.0 | 100.26 | N |
| 88 | $123^{+5}_{-5}$ | $41^{+2}_{-2}$ | $164^{+6}_{-6}$ | 0.33 | $2.18^{+0.39}_{-0.33}$ | $0.4^{+0.06}_{-0.05}$ | 0.62 | 0.0 | 0.0 | 99.08 | N |
| 89 | $128^{+0}_{0}$ | $43^{+0}_{0}$ | $171^{+0}_{0}$ | 0.33 | $1.64^{+0.0}_{0.0}$ | $0.31^{+0.0}_{0.0}$ | 0.67 | 0.0 | 0.0 | 98.01 | N |
| 90 | $129^{+6}_{-7}$ | $43^{+2}_{-2}$ | $172^{+8}_{-9}$ | 0.33 | $1.44^{+0.26}_{-0.36}$ | $0.28^{+0.04}_{-0.06}$ | 0.71 | 0.0 | 0.0 | 96.62 | N |
| 91 | $131^{+6}_{-10}$ | $44^{+2}_{-3}$ | $175^{+7}_{-14}$ | 0.33 | $1.17^{+0.29}_{-0.33}$ | $0.23^{+0.05}_{-0.06}$ | 0.75 | 0.0 | 0.0 | 95.44 | N |
| 92 | $132^{+0}_{0}$ | $44^{+0}_{0}$ | $176^{+0}_{0}$ | 0.33 | $0.95^{+0.0}_{0.0}$ | $0.19^{+0.0}_{0.0}$ | 0.79 | −0.0 | 0.0 | 94.49 | N |
| 93 | $131^{+7}_{-3}$ | $44^{+2}_{-1}$ | $175^{+10}_{-4}$ | 0.33 | $0.53^{+0.38}_{-0.13}$ | $0.11^{+0.07}_{-0.03}$ | 0.82 | −0.0 | 0.0 | 94.81 | N |
| 94 | $135^{+6}_{-7}$ | $45^{+2}_{-2}$ | $180^{+8}_{-10}$ | 0.33 | $0.48^{+0.23}_{-0.27}$ | $0.1^{+0.04}_{-0.06}$ | 0.86 | 0.0 | 0.0 | 95.9 | N |
| 95 | $133^{+9}_{-3}$ | $44^{+3}_{-1}$ | $177^{+12}_{-5}$ | 0.33 | $0.48^{+0.12}_{-0.19}$ | $0.1^{+0.02}_{-0.04}$ | 0.89 | 0.0 | 0.0 | 94.04 | N |
| 96 | $138^{+5}_{-8}$ | $46^{+2}_{-3}$ | $184^{+7}_{-11}$ | 0.33 | $0.28^{+0.05}_{-0.1}$ | $0.06^{+0.01}_{-0.02}$ | 0.95 | 0.0 | 0.0 | 90.16 | N |
| 97 | $149^{+0}_{-9}$ | $50^{+0}_{-3}$ | $198^{+0}_{-12}$ | 0.33 | $0.15^{+0.08}_{0.0}$ | $0.04^{+0.02}_{0.0}$ | 0.96 | 0.0 | 0.0 | 89.33 | N |
| 98 | $138^{+8}_{-15}$ | $46^{+3}_{-5}$ | $184^{+11}_{-20}$ | 0.33 | $0.22^{+0.33}_{-0.13}$ | $0.05^{+0.07}_{-0.03}$ | 0.98 | 0.0 | 0.0 | 86.4 | Y |
| 99 | $128^{+11}_{-8}$ | $43^{+4}_{-3}$ | $170^{+15}_{-11}$ | 0.33 | $0.53^{+0.18}_{-0.12}$ | $0.11^{+0.04}_{-0.02}$ | 0.99 | 0.0 | 0.0 | 78.58 | N |
| 100 | $97^{+9}_{-6}$ | $48^{+5}_{-3}$ | $145^{+14}_{-9}$ | 0.5 | $4.13^{+1.16}_{-0.98}$ | $0.68^{+0.15}_{-0.14}$ | 0.18 | 0.0 | 0.0 | 96.91 | N |
| 101 | $94^{+9}_{-3}$ | $47^{+5}_{-1}$ | $141^{+14}_{-4}$ | 0.5 | $4.57^{+0.09}_{-1.15}$ | $0.74^{+0.01}_{-0.16}$ | 0.33 | −0.0 | 0.0 | 97.82 | N |
| 102 | $95^{+9}_{-3}$ | $47^{+5}_{-1}$ | $142^{+14}_{-4}$ | 0.5 | $4.52^{+0.58}_{-1.19}$ | $0.74^{+0.08}_{-0.16}$ | 0.4 | 0.0 | 0.0 | 96.11 | N |
| 103 | $100^{+6}_{-10}$ | $50^{+3}_{-5}$ | $150^{+9}_{-14}$ | 0.5 | $4.11^{+1.02}_{-0.67}$ | $0.68^{+0.13}_{-0.09}$ | 0.43 | 0.0 | 0.0 | 98.08 | N |
| 104 | $92^{+9}_{-8}$ | $46^{+5}_{-4}$ | $138^{+14}_{-12}$ | 0.5 | $4.65^{+1.42}_{-1.15}$ | $0.75^{+0.18}_{-0.16}$ | 0.46 | 0.0 | 0.0 | 89.61 | N |
| 105 | $85^{+12}_{-7}$ | $43^{+6}_{-3}$ | $128^{+18}_{-10}$ | 0.5 | $4.85^{+1.05}_{-1.44}$ | $0.78^{+0.14}_{-0.19}$ | 0.5 | −0.0 | 0.0 | 90.87 | N |
| 106 | $93^{+8}_{-5}$ | $46^{+4}_{-2}$ | $139^{+13}_{-7}$ | 0.5 | $4.94^{+0.72}_{-1.07}$ | $0.79^{+0.09}_{-0.14}$ | 0.52 | 0.0 | 0.0 | 100.84 | N |
| 107 | $102^{+4}_{-7}$ | $51^{+2}_{-3}$ | $152^{+5}_{-10}$ | 0.5 | $4.08^{+0.9}_{-0.66}$ | $0.68^{+0.16}_{-0.05}$ | 0.55 | 0.0 | 0.0 | 102.35 | N |
| 108 | $104^{+4}_{-7}$ | $52^{+2}_{-3}$ | $157^{+6}_{-10}$ | 0.5 | $3.97^{+0.62}_{-0.76}$ | $0.66^{+0.08}_{-0.11}$ | 0.57 | 0.0 | 0.0 | 101.69 | Y |
| 109 | $107^{+3}_{-6}$ | $53^{+2}_{-3}$ | $160^{+5}_{-9}$ | 0.5 | $3.04^{+1.14}_{-0.26}$ | $0.53^{+0.16}_{-0.04}$ | 0.59 | 0.0 | 0.0 | 101.47 | N |
| 110 | $109^{+11}_{-5}$ | $55^{+6}_{-2}$ | $164^{+17}_{-7}$ | 0.5 | $2.77^{+0.61}_{-1.07}$ | $0.49^{+0.09}_{-0.17}$ | 0.62 | −0.0 | 0.0 | 100.92 | N |
| 111 | $109^{+8}_{-3}$ | $55^{+4}_{-1}$ | $164^{+12}_{-4}$ | 0.5 | $2.79^{+0.0}_{-0.89}$ | $0.49^{+0.0}_{-0.14}$ | 0.67 | 0.0 | 0.0 | 99.49 | N |

| | | | | | | | | | | | |
|---|---|---|---|---|---|---|---|---|---|---|---|
| 112 | $117^{+9}_{-6}$ | $59^{+4}_{-3}$ | $176^{+13}_{-10}$ | 0.5 | $1.59^{+0.53}_{-0.82}$ | $0.31^{+0.09}_{-0.14}$ | 0.71 | 0.0 | 0.0 | 97.88 | N |
| 113 | $121^{+8}_{-8}$ | $60^{+4}_{-4}$ | $181^{+12}_{-12}$ | 0.5 | $1.22^{+0.46}_{-0.48}$ | $0.24^{+0.08}_{-0.09}$ | 0.75 | 0.0 | 0.0 | 97.82 | N |
| 114 | $122^{+9}_{-8}$ | $61^{+4}_{-4}$ | $182^{+13}_{-11}$ | 0.5 | $0.8^{+0.45}_{-0.38}$ | $0.17^{+0.08}_{-0.07}$ | 0.79 | $-0.0$ | 0.0 | 98.79 | N |
| 115 | $121^{+7}_{-7}$ | $61^{+4}_{-4}$ | $182^{+11}_{-11}$ | 0.5 | $0.7^{+0.25}_{-0.37}$ | $0.15^{+0.05}_{-0.07}$ | 0.82 | $-0.0$ | 0.0 | 97.5 | N |
| 116 | $123^{+5}_{-7}$ | $62^{+2}_{-4}$ | $185^{+7}_{-11}$ | 0.5 | $0.75^{+0.04}_{-0.42}$ | $0.16^{+0.01}_{-0.08}$ | 0.86 | 0.0 | 0.0 | 97.48 | N |
| 117 | $122^{+23}_{-9}$ | $61^{+12}_{-4}$ | $183^{+35}_{-13}$ | 0.5 | $0.44^{+0.27}_{-0.29}$ | $0.1^{+0.05}_{-0.06}$ | 0.89 | 0.0 | 0.0 | 95.6 | N |
| 118 | $122^{+14}_{-5}$ | $61^{+7}_{-3}$ | $184^{+21}_{-8}$ | 0.5 | $0.28^{+0.12}_{-0.08}$ | $0.06^{+0.02}_{-0.02}$ | 0.95 | 0.0 | 0.0 | 92.64 | N |
| 119 | $126^{+4}_{-10}$ | $63^{+2}_{-5}$ | $190^{+6}_{-15}$ | 0.5 | $0.23^{+0.07}_{-0.07}$ | $0.05^{+0.01}_{-0.02}$ | 0.96 | 0.0 | 0.0 | 89.96 | N |
| 120 | $123^{+19}_{-12}$ | $61^{+10}_{-6}$ | $184^{+29}_{-18}$ | 0.5 | $0.17^{+0.45}_{-0.12}$ | $0.04^{+0.09}_{-0.03}$ | 0.98 | 0.0 | 0.0 | 86.49 | Y |
| 121 | $112^{+8}_{-9}$ | $56^{+4}_{-4}$ | $168^{+12}_{-13}$ | 0.5 | $0.64^{+0.15}_{-0.22}$ | $0.14^{+0.03}_{-0.04}$ | 0.99 | 0.0 | 0.0 | 78.83 | N |
| 122 | $98^{+5}_{-8}$ | $59^{+3}_{-5}$ | $157^{+8}_{-13}$ | 0.6 | $3.96^{+0.85}_{-0.89}$ | $0.66^{+0.11}_{-0.12}$ | 0.57 | $-0.0$ | 0.0 | 101.81 | Y |
| 123 | $105^{+10}_{-4}$ | $63^{+6}_{-2}$ | $167^{+16}_{-6}$ | 0.6 | $2.56^{+0.45}_{-1.1}$ | $0.46^{+0.07}_{-0.18}$ | 0.67 | 0.0 | 0.0 | 99.83 | N |
| 124 | $112^{+11}_{-6}$ | $67^{+6}_{-4}$ | $179^{+17}_{-9}$ | 0.6 | $1.29^{+0.38}_{-0.71}$ | $0.25^{+0.06}_{-0.13}$ | 0.75 | 0.0 | 0.0 | 99.3 | N |
| 125 | $117^{+8}_{-8}$ | $70^{+5}_{-5}$ | $187^{+13}_{-13}$ | 0.6 | $0.36^{+0.15}_{-0.26}$ | $0.08^{+0.03}_{-0.06}$ | 0.92 | 0.0 | 0.0 | 96.66 | N |
| 126 | $83^{+9}_{-9}$ | $58^{+6}_{-6}$ | $141^{+15}_{-15}$ | 0.7 | $5.09^{+1.82}_{-1.43}$ | $0.81^{+0.23}_{-0.19}$ | 0.46 | 0.0 | 0.0 | 88.97 | N |
| 127 | $71^{+15}_{-12}$ | $50^{+10}_{-9}$ | $121^{+25}_{-21}$ | 0.7 | $4.3^{+2.23}_{-2.22}$ | $0.7^{+0.29}_{-0.32}$ | 0.5 | 0.0 | 0.0 | 82.65 | N |
| 128 | $80^{+10}_{-7}$ | $56^{+7}_{-5}$ | $136^{+18}_{-11}$ | 0.7 | $5.82^{+1.4}_{-1.72}$ | $0.9^{+0.17}_{-0.22}$ | 0.52 | 0.0 | 0.0 | 100.27 | N |
| 129 | $85^{+7}_{-5}$ | $59^{+5}_{-3}$ | $144^{+12}_{-8}$ | 0.7 | $5.02^{+1.12}_{-1.07}$ | $0.8^{+0.14}_{-0.14}$ | 0.55 | 0.0 | 0.0 | 102.34 | N |
| 130 | $90^{+6}_{-7}$ | $63^{+4}_{-5}$ | $153^{+10}_{-12}$ | 0.7 | $4.47^{+0.8}_{-1.14}$ | $0.73^{+0.1}_{-0.16}$ | 0.57 | 0.0 | 0.0 | 102.21 | N |
| 131 | $93^{+0}_{0}$ | $65^{+0}_{0}$ | $158^{+0}_{0}$ | 0.7 | $3.84^{+0.0}_{0.0}$ | $0.64^{+0.0}_{0.0}$ | 0.59 | 0.0 | 0.0 | 101.68 | N |
| 132 | $96^{+8}_{-9}$ | $67^{+5}_{-6}$ | $163^{+13}_{-15}$ | 0.7 | $3.39^{+0.77}_{-1.09}$ | $0.58^{+0.11}_{-0.16}$ | 0.62 | 0.0 | 0.0 | 100.87 | N |
| 133 | $100^{+4}_{-5}$ | $70^{+3}_{-4}$ | $169^{+7}_{-9}$ | 0.7 | $2.48^{+0.64}_{-0.32}$ | $0.45^{+0.1}_{-0.05}$ | 0.67 | 0.0 | 0.0 | 99.13 | N |
| 134 | $105^{+13}_{-7}$ | $74^{+9}_{-5}$ | $179^{+22}_{-12}$ | 0.7 | $1.72^{+0.91}_{-0.76}$ | $0.33^{+0.14}_{-0.13}$ | 0.71 | 0.0 | 0.0 | 99.03 | N |
| 135 | $106^{+10}_{-6}$ | $74^{+7}_{-4}$ | $180^{+17}_{-11}$ | 0.7 | $1.39^{+0.34}_{-0.73}$ | $0.27^{+0.06}_{-0.13}$ | 0.75 | 0.0 | 0.0 | 99.19 | N |
| 136 | $112^{+9}_{-6}$ | $78^{+6}_{-4}$ | $190^{+15}_{-10}$ | 0.7 | $0.61^{+0.47}_{-0.23}$ | $0.13^{+0.09}_{-0.05}$ | 0.79 | 0.0 | 0.0 | 99.55 | N |
| 137 | $113^{+6}_{-7}$ | $79^{+4}_{-5}$ | $192^{+10}_{-12}$ | 0.7 | $0.51^{+0.33}_{-0.15}$ | $0.11^{+0.06}_{-0.03}$ | 0.82 | 0.0 | 0.0 | 100.23 | N |
| 138 | $114^{+6}_{-9}$ | $80^{+4}_{-6}$ | $193^{+11}_{-15}$ | 0.7 | $0.4^{+0.24}_{-0.17}$ | $0.09^{+0.05}_{-0.04}$ | 0.86 | 0.0 | 0.0 | 99.5 | N |
| 139 | $113^{+7}_{-11}$ | $79^{+5}_{-7}$ | $192^{+12}_{-18}$ | 0.7 | $0.3^{+0.27}_{-0.15}$ | $0.07^{+0.06}_{-0.03}$ | 0.89 | 0.0 | 0.0 | 98.79 | N |
| 140 | $112^{+6}_{-6}$ | $78^{+4}_{-4}$ | $190^{+11}_{-11}$ | 0.7 | $0.24^{+0.27}_{-0.1}$ | $0.05^{+0.06}_{-0.02}$ | 0.92 | 0.0 | 0.0 | 96.11 | N |
| 141 | $108^{+7}_{-2}$ | $76^{+5}_{-2}$ | $184^{+11}_{-4}$ | 0.7 | $0.26^{+0.13}_{-0.08}$ | $0.06^{+0.03}_{-0.02}$ | 0.95 | 0.0 | 0.0 | 95.19 | N |
| 142 | $109^{+7}_{-2}$ | $76^{+5}_{-2}$ | $185^{+11}_{-4}$ | 0.7 | $0.24^{+0.07}_{-0.09}$ | $0.05^{+0.01}_{-0.02}$ | 0.96 | 0.0 | 0.0 | 92.5 | N |
| 143 | $116^{+9}_{-12}$ | $81^{+6}_{-9}$ | $198^{+15}_{-21}$ | 0.7 | $0.11^{+0.33}_{-0.08}$ | $0.02^{+0.07}_{-0.02}$ | 0.98 | 0.0 | 0.0 | 89.74 | N |
| 144 | $98^{+7}_{-7}$ | $69^{+5}_{-5}$ | $167^{+12}_{-11}$ | 0.7 | $0.67^{+0.2}_{-0.22}$ | $0.14^{+0.04}_{-0.04}$ | 0.99 | 0.0 | 0.0 | 78.96 | Y |
| 145 | $79^{+7}_{-9}$ | $64^{+5}_{-7}$ | $143^{+12}_{-17}$ | 0.8 | $4.97^{+1.74}_{-1.18}$ | $0.79^{+0.22}_{-0.16}$ | 0.46 | 0.0 | 0.0 | 89.2 | N |
| 146 | $70^{+1}_{-12}$ | $56^{+1}_{-10}$ | $126^{+2}_{-22}$ | 0.8 | $2.86^{+2.46}_{-0.22}$ | $0.5^{+0.33}_{-0.03}$ | 0.5 | 0.0 | 0.0 | 81.64 | N |
| 147 | $76^{+8}_{-7}$ | $61^{+7}_{-5}$ | $137^{+15}_{-12}$ | 0.8 | $6.08^{+1.62}_{-1.34}$ | $0.93^{+0.2}_{-0.17}$ | 0.52 | 0.0 | 0.0 | 100.3 | N |
| 148 | $81^{+7}_{-4}$ | $65^{+6}_{-3}$ | $145^{+13}_{-8}$ | 0.8 | $5.34^{+0.84}_{-1.07}$ | $0.84^{+0.11}_{-0.14}$ | 0.55 | 0.0 | 0.0 | 101.96 | N |
| 149 | $85^{+6}_{-7}$ | $68^{+4}_{-5}$ | $153^{+10}_{-12}$ | 0.8 | $4.72^{+0.98}_{-1.09}$ | $0.76^{+0.13}_{-0.15}$ | 0.57 | 0.0 | 0.0 | 102.15 | N |
| 150 | $85^{+11}_{-4}$ | $68^{+9}_{-4}$ | $153^{+20}_{-8}$ | 0.8 | $4.49^{+0.71}_{-1.44}$ | $0.73^{+0.12}_{-0.17}$ | 0.59 | 0.0 | 0.0 | 101.76 | N |
| 151 | $88^{+8}_{-3}$ | $70^{+6}_{-3}$ | $158^{+14}_{-6}$ | 0.8 | $3.65^{+0.77}_{-0.75}$ | $0.62^{+0.1}_{-0.11}$ | 0.62 | 0.0 | 0.0 | 100.51 | N |
| 152 | $95^{+12}_{-6}$ | $76^{+9}_{-5}$ | $170^{+21}_{-11}$ | 0.8 | $2.57^{+0.83}_{-0.97}$ | $0.46^{+0.12}_{-0.15}$ | 0.67 | 0.0 | 0.0 | 99.16 | N |
| 153 | $99^{+10}_{-8}$ | $79^{+8}_{-6}$ | $178^{+17}_{-14}$ | 0.8 | $1.92^{+0.65}_{-0.96}$ | $0.36^{+0.1}_{-0.16}$ | 0.71 | 0.0 | 0.0 | 99.03 | N |
| 154 | $100^{+9}_{0}$ | $80^{+8}_{0}$ | $180^{+17}_{0}$ | 0.8 | $1.11^{+0.18}_{-0.38}$ | $0.22^{+0.03}_{-0.07}$ | 0.75 | 0.0 | 0.0 | 99.91 | N |
| 155 | $107^{+8}_{-8}$ | $86^{+6}_{-6}$ | $193^{+14}_{-14}$ | 0.8 | $0.54^{+0.34}_{-0.2}$ | $0.12^{+0.07}_{-0.04}$ | 0.82 | 0.0 | 0.0 | 100.15 | N |
| 156 | $108^{+7}_{-7}$ | $87^{+5}_{-6}$ | $195^{+12}_{-13}$ | 0.8 | $0.39^{+0.2}_{-0.15}$ | $0.09^{+0.04}_{-0.03}$ | 0.86 | 0.0 | 0.0 | 100.91 | N |
| 157 | $109^{+6}_{-8}$ | $87^{+5}_{-6}$ | $196^{+10}_{-14}$ | 0.8 | $0.31^{+0.26}_{-0.11}$ | $0.07^{+0.05}_{-0.02}$ | 0.89 | 0.0 | 0.0 | 98.3 | N |
| 158 | $108^{+7}_{-9}$ | $86^{+5}_{-7}$ | $194^{+12}_{-16}$ | 0.8 | $0.22^{+0.16}_{-0.14}$ | $0.05^{+0.03}_{-0.03}$ | 0.92 | 0.0 | 0.0 | 99.49 | N |
| 159 | $109^{+5}_{-8}$ | $87^{+4}_{-7}$ | $196^{+9}_{-15}$ | 0.8 | $0.32^{+0.04}_{-0.26}$ | $0.07^{+0.01}_{-0.06}$ | 0.95 | 0.0 | 0.0 | 95.73 | Y |
| 160 | $105^{+4}_{-5}$ | $84^{+3}_{-4}$ | $188^{+8}_{-9}$ | 0.8 | $0.23^{+0.06}_{-0.15}$ | $0.05^{+0.01}_{-0.03}$ | 0.96 | 0.0 | 0.0 | 93.11 | N |
| 161 | $104^{+7}_{-8}$ | $84^{+6}_{-7}$ | $188^{+13}_{-15}$ | 0.8 | $0.15^{+0.44}_{-0.07}$ | $0.04^{+0.09}_{-0.02}$ | 0.98 | 0.0 | 0.0 | 89.89 | N |
| 162 | $92^{+7}_{-7}$ | $74^{+6}_{-5}$ | $166^{+13}_{-12}$ | 0.8 | $0.7^{+0.14}_{-0.29}$ | $0.15^{+0.03}_{-0.06}$ | 0.99 | 0.0 | 0.0 | 78.08 | N |
| 163 | $70^{+9}_{-7}$ | $63^{+8}_{-6}$ | $134^{+17}_{-13}$ | 0.9 | $5.91^{+1.67}_{-1.53}$ | $0.91^{+0.2}_{-0.2}$ | 0.46 | 0.0 | 0.0 | 87.88 | N |
| 164 | $58^{+11}_{-10}$ | $52^{+9}_{-9}$ | $110^{+20}_{-19}$ | 0.9 | $3.67^{+2.88}_{-1.84}$ | $0.62^{+0.37}_{-0.27}$ | 0.5 | 0.0 | 0.0 | 81.63 | N |
| 165 | $72^{+6}_{-7}$ | $65^{+5}_{-6}$ | $137^{+11}_{-13}$ | 0.9 | $6.16^{+1.37}_{-1.18}$ | $0.94^{+0.17}_{-0.15}$ | 0.52 | 0.0 | 0.0 | 98.6 | N |
| 166 | $75^{+7}_{-6}$ | $68^{+7}_{-5}$ | $143^{+14}_{-11}$ | 0.9 | $5.75^{+1.25}_{-1.28}$ | $0.89^{+0.15}_{-0.16}$ | 0.55 | 0.0 | 0.0 | 101.48 | N |
| 167 | $78^{+9}_{-3}$ | $70^{+8}_{-3}$ | $148^{+17}_{-6}$ | 0.9 | $5.25^{+0.5}_{-1.69}$ | $0.83^{+0.06}_{-0.23}$ | 0.57 | 0.0 | 0.0 | 100.99 | N |
| 168 | $83^{+7}_{-7}$ | $75^{+7}_{-7}$ | $157^{+14}_{-14}$ | 0.9 | $4.35^{+1.04}_{-1.14}$ | $0.71^{+0.14}_{-0.16}$ | 0.59 | 0.0 | 0.0 | 100.91 | N |
| 169 | $81^{+10}_{-1}$ | $73^{+9}_{-1}$ | $153^{+19}_{-2}$ | 0.9 | $4.47^{+0.19}_{-1.37}$ | $0.73^{+0.03}_{-0.19}$ | 0.62 | 0.0 | 0.0 | 99.4 | N |

| | | | | | | | | | | | |
|---|---|---|---|---|---|---|---|---|---|---|---|
| 170 | $91^{+9}_{-7}$ | $81^{+8}_{-6}$ | $172^{+17}_{-13}$ | 0.9 | $2.62^{+1.14}_{-0.8}$ | $0.47^{+0.16}_{-0.12}$ | 0.67 | 0.0 | 0.0 | 98.65 | N |
| 171 | $92^{+10}_{-8}$ | $83^{+9}_{-7}$ | $175^{+18}_{-16}$ | 0.9 | $2.1^{+0.76}_{-0.95}$ | $0.39^{+0.12}_{-0.16}$ | 0.71 | 0.0 | 0.0 | 99.02 | N |
| 172 | $99^{+7}_{-9}$ | $89^{+7}_{-8}$ | $189^{+14}_{-17}$ | 0.9 | $1.07^{+0.85}_{-0.35}$ | $0.22^{+0.14}_{-0.07}$ | 0.75 | 0.0 | 0.0 | 99.33 | N |
| 173 | $101^{+9}_{-5}$ | $91^{+8}_{-4}$ | $192^{+18}_{-9}$ | 0.9 | $0.77^{+0.37}_{-0.31}$ | $0.16^{+0.07}_{-0.06}$ | 0.79 | 0.0 | 0.0 | 99.6 | N |
| 174 | $102^{+7}_{-4}$ | $92^{+7}_{-4}$ | $194^{+14}_{-8}$ | 0.9 | $0.58^{+0.16}_{-0.21}$ | $0.12^{+0.03}_{-0.04}$ | 0.82 | 0.0 | 0.0 | 99.42 | N |
| 175 | $105^{+5}_{-6}$ | $95^{+5}_{-5}$ | $200^{+10}_{-10}$ | 0.9 | $0.37^{+0.13}_{-0.14}$ | $0.08^{+0.03}_{-0.03}$ | 0.86 | 0.0 | 0.0 | 100.74 | N |
| 176 | $98^{+10}_{-3}$ | $88^{+9}_{-3}$ | $186^{+19}_{-6}$ | 0.9 | $0.46^{+0.01}_{-0.28}$ | $0.1^{+0.0}_{-0.06}$ | 0.89 | 0.0 | 0.0 | 99.6 | N |
| 177 | $104^{+6}_{-9}$ | $93^{+5}_{-8}$ | $197^{+11}_{-18}$ | 0.9 | $0.2^{+0.23}_{-0.11}$ | $0.05^{+0.05}_{-0.02}$ | 0.92 | 0.0 | 0.0 | 98.46 | N |
| 178 | $99^{+0}_{0}$ | $89^{+0}_{0}$ | $188^{+0}_{0}$ | 0.9 | $0.28^{+0.0}_{0.0}$ | $0.06^{+0.0}_{0.0}$ | 0.95 | 0.0 | 0.0 | 97.72 | N |
| 179 | $100^{+8}_{-7}$ | $90^{+7}_{-6}$ | $190^{+14}_{-13}$ | 0.9 | $0.21^{+0.08}_{-0.18}$ | $0.05^{+0.02}_{-0.04}$ | 0.96 | 0.0 | 0.0 | 95.52 | N |
| 180 | $99^{+7}_{-9}$ | $89^{+6}_{-8}$ | $188^{+13}_{-18}$ | 0.9 | $0.15^{+0.5}_{-0.11}$ | $0.03^{+0.1}_{-0.02}$ | 0.98 | 0.0 | 0.0 | 89.93 | N |
| 181 | $89^{+6}_{-6}$ | $80^{+5}_{-5}$ | $168^{+11}_{-11}$ | 0.9 | $0.6^{+0.37}_{-0.18}$ | $0.13^{+0.07}_{-0.04}$ | 0.99 | 0.0 | 0.0 | 82.66 | Y |
| 182 | $71^{+7}_{-5}$ | $71^{+7}_{-5}$ | $143^{+14}_{-11}$ | 1.0 | $5.32^{+1.04}_{-1.07}$ | $0.84^{+0.13}_{-0.14}$ | 0.18 | 0.0 | 0.0 | 94.63 | N |
| 183 | $71^{+7}_{-6}$ | $71^{+7}_{-6}$ | $142^{+14}_{-12}$ | 1.0 | $5.29^{+1.06}_{-1.15}$ | $0.84^{+0.13}_{-0.15}$ | 0.26 | 0.0 | 0.0 | 93.49 | N |
| 184 | $71^{+5}_{-8}$ | $71^{+5}_{-8}$ | $142^{+10}_{-16}$ | 1.0 | $5.32^{+1.55}_{-0.9}$ | $0.84^{+0.19}_{-0.12}$ | 0.31 | 0.0 | 0.0 | 93.75 | N |
| 185 | $70^{+5}_{-6}$ | $70^{+5}_{-6}$ | $141^{+11}_{-12}$ | 1.0 | $5.44^{+1.17}_{-0.99}$ | $0.85^{+0.15}_{-0.13}$ | 0.33 | 0.0 | 0.0 | 94.49 | N |
| 186 | $70^{+7}_{-8}$ | $70^{+7}_{-8}$ | $140^{+13}_{-15}$ | 1.0 | $5.53^{+1.19}_{-1.62}$ | $0.87^{+0.18}_{-0.18}$ | 0.36 | 0.0 | 0.0 | 93.8 | N |
| 187 | $70^{+6}_{-6}$ | $70^{+6}_{-6}$ | $141^{+13}_{-12}$ | 1.0 | $5.64^{+0.98}_{-1.49}$ | $0.88^{+0.15}_{-0.17}$ | 0.37 | 0.0 | 0.0 | 91.04 | N |
| 188 | $74^{+5}_{-7}$ | $74^{+5}_{-7}$ | $147^{+10}_{-14}$ | 1.0 | $5.0^{+1.11}_{-0.88}$ | $0.8^{+0.14}_{-0.12}$ | 0.39 | 0.0 | 0.0 | 95.1 | N |
| 189 | $73^{+6}_{-6}$ | $73^{+6}_{-6}$ | $145^{+13}_{-12}$ | 1.0 | $5.2^{+1.16}_{-1.23}$ | $0.82^{+0.15}_{-0.16}$ | 0.4 | 0.0 | 0.0 | 96.5 | N |
| 190 | $69^{+6}_{-6}$ | $69^{+6}_{-6}$ | $139^{+13}_{-13}$ | 1.0 | $5.61^{+1.25}_{-1.19}$ | $0.88^{+0.15}_{-0.15}$ | 0.41 | 0.0 | 0.0 | 91.33 | N |
| 191 | $72^{+10}_{-3}$ | $72^{+10}_{-3}$ | $145^{+19}_{-6}$ | 1.0 | $5.16^{+0.73}_{-1.24}$ | $0.82^{+0.09}_{-0.16}$ | 0.43 | 0.0 | 0.0 | 95.01 | N |
| 192 | $70^{+6}_{-7}$ | $70^{+6}_{-7}$ | $139^{+11}_{-14}$ | 1.0 | $5.85^{+1.06}_{-1.42}$ | $0.91^{+0.13}_{-0.18}$ | 0.44 | 0.0 | 0.0 | 93.43 | N |
| 193 | $75^{+3}_{-8}$ | $75^{+3}_{-8}$ | $150^{+6}_{-15}$ | 1.0 | $4.76^{+1.16}_{-0.94}$ | $0.77^{+0.15}_{-0.13}$ | 0.45 | 0.0 | 0.0 | 97.02 | N |
| 194 | $67^{+7}_{-6}$ | $67^{+7}_{-6}$ | $135^{+14}_{-13}$ | 1.0 | $6.0^{+1.38}_{-1.39}$ | $0.92^{+0.17}_{-0.18}$ | 0.46 | 0.0 | 0.0 | 88.07 | N |
| 195 | $69^{+7}_{-7}$ | $69^{+7}_{-7}$ | $137^{+14}_{-14}$ | 1.0 | $5.75^{+1.13}_{-1.66}$ | $0.89^{+0.18}_{-0.18}$ | 0.47 | 0.0 | 0.0 | 94.82 | N |
| 196 | $75^{+6}_{-6}$ | $75^{+6}_{-6}$ | $150^{+11}_{-11}$ | 1.0 | $5.33^{+0.97}_{-1.13}$ | $0.84^{+0.12}_{-0.15}$ | 0.48 | 0.0 | 0.0 | 90.2 | N |
| 197 | $58^{+9}_{-9}$ | $58^{+9}_{-9}$ | $115^{+18}_{-19}$ | 1.0 | $3.82^{+2.82}_{-2.19}$ | $0.64^{+0.36}_{-0.33}$ | 0.5 | 0.0 | 0.0 | 82.35 | N |
| 198 | $65^{+8}_{-5}$ | $65^{+8}_{-5}$ | $130^{+17}_{-10}$ | 1.0 | $6.38^{+1.19}_{-1.92}$ | $0.97^{+0.14}_{-0.24}$ | 0.51 | 0.0 | 0.0 | 94.1 | N |
| 199 | $69^{+7}_{-6}$ | $69^{+7}_{-6}$ | $137^{+15}_{-11}$ | 1.0 | $6.23^{+1.16}_{-1.47}$ | $0.95^{+0.14}_{-0.19}$ | 0.52 | 0.0 | 0.0 | 98.66 | N |
| 200 | $70^{+6}_{-6}$ | $70^{+6}_{-6}$ | $141^{+12}_{-13}$ | 1.0 | $6.0^{+1.34}_{-1.13}$ | $0.92^{+0.16}_{-0.14}$ | 0.53 | 0.0 | 0.0 | 100.16 | N |
| 201 | $72^{+6}_{-6}$ | $72^{+6}_{-6}$ | $144^{+11}_{-13}$ | 1.0 | $5.61^{+1.15}_{-1.07}$ | $0.88^{+0.14}_{-0.14}$ | 0.55 | 0.0 | 0.0 | 100.98 | N |
| 202 | $74^{+7}_{-5}$ | $74^{+7}_{-5}$ | $149^{+14}_{-10}$ | 1.0 | $5.25^{+0.87}_{-1.29}$ | $0.83^{+0.11}_{-0.17}$ | 0.57 | 0.0 | 0.0 | 100.74 | N |
| 203 | $77^{+7}_{-8}$ | $77^{+7}_{-8}$ | $155^{+14}_{-16}$ | 1.0 | $4.46^{+1.15}_{-1.03}$ | $0.73^{+0.15}_{-0.14}$ | 0.59 | 0.0 | 0.0 | 100.32 | N |
| 204 | $80^{+7}_{-7}$ | $80^{+7}_{-7}$ | $161^{+14}_{-14}$ | 1.0 | $3.76^{+1.28}_{-0.88}$ | $0.63^{+0.17}_{-0.13}$ | 0.62 | 0.0 | 0.0 | 99.15 | N |
| 205 | $84^{+8}_{-8}$ | $84^{+8}_{-8}$ | $168^{+16}_{-15}$ | 1.0 | $2.84^{+1.15}_{-0.82}$ | $0.5^{+0.16}_{-0.13}$ | 0.67 | 0.0 | 0.0 | 97.84 | N |
| 206 | $89^{+9}_{-9}$ | $89^{+9}_{-9}$ | $178^{+18}_{-17}$ | 1.0 | $1.99^{+0.88}_{-0.91}$ | $0.37^{+0.13}_{-0.15}$ | 0.71 | 0.0 | 0.0 | 97.97 | N |
| 207 | $93^{+8}_{-9}$ | $93^{+8}_{-9}$ | $186^{+17}_{-17}$ | 1.0 | $1.2^{+0.92}_{-0.45}$ | $0.24^{+0.15}_{-0.08}$ | 0.75 | 0.0 | 0.0 | 98.49 | N |
| 208 | $96^{+7}_{-5}$ | $96^{+7}_{-5}$ | $192^{+14}_{-10}$ | 1.0 | $0.81^{+0.22}_{-0.36}$ | $0.17^{+0.04}_{-0.07}$ | 0.79 | 0.0 | 0.0 | 99.07 | N |
| 209 | $98^{+6}_{-4}$ | $98^{+6}_{-4}$ | $196^{+13}_{-8}$ | 1.0 | $0.64^{+0.09}_{-0.27}$ | $0.14^{+0.02}_{-0.05}$ | 0.82 | 0.0 | 0.0 | 99.23 | N |
| 210 | $98^{+6}_{-7}$ | $98^{+6}_{-7}$ | $196^{+13}_{-14}$ | 1.0 | $0.41^{+0.27}_{-0.2}$ | $0.09^{+0.05}_{-0.04}$ | 0.86 | 0.0 | 0.0 | 99.87 | N |
| 211 | $102^{+1}_{-4}$ | $102^{+1}_{-4}$ | $204^{+2}_{-7}$ | 1.0 | $0.25^{+0.04}_{-0.06}$ | $0.06^{+0.01}_{-0.01}$ | 0.89 | 0.0 | 0.0 | 99.07 | N |
| 212 | $98^{+7}_{-8}$ | $98^{+7}_{-8}$ | $197^{+13}_{-15}$ | 1.0 | $0.19^{+0.22}_{-0.11}$ | $0.04^{+0.05}_{-0.02}$ | 0.92 | 0.0 | 0.0 | 98.6 | N |
| 213 | $106^{+0}_{-12}$ | $106^{+0}_{-12}$ | $213^{+0}_{-25}$ | 1.0 | $0.05^{+0.21}_{0.0}$ | $0.01^{+0.05}_{0.0}$ | 0.95 | 0.0 | 0.0 | 97.02 | N |
| 214 | $94^{+5}_{-3}$ | $94^{+5}_{-3}$ | $189^{+11}_{-7}$ | 1.0 | $0.2^{+0.12}_{-0.12}$ | $0.05^{+0.03}_{-0.03}$ | 0.96 | 0.0 | 0.0 | 93.56 | N |
| 215 | $96^{+4}_{-5}$ | $96^{+4}_{-5}$ | $193^{+7}_{-9}$ | 1.0 | $0.1^{+0.08}_{-0.05}$ | $0.02^{+0.02}_{-0.01}$ | 0.98 | 0.0 | 0.0 | 90.9 | N |
| 216 | $84^{+4}_{-9}$ | $84^{+4}_{-9}$ | $169^{+8}_{-19}$ | 1.0 | $0.64^{+0.25}_{-0.25}$ | $0.14^{+0.05}_{-0.05}$ | 0.99 | 0.0 | 0.0 | 78.41 | Y |
| **Head-on eBBH runs** | | | | | | | | | | | |
| 1 | $96^{+8}_{0}$ | $96^{+8}_{0}$ | $193^{+16}_{0}$ | 1.0 | $0.4^{+0.0}_{-0.13}$ | $0.09^{+0.0}_{-0.03}$ | 1.0 | 0.7 | 0.0 | 98.43 | Y |
| 2 | $97^{+2}_{-6}$ | $97^{+2}_{-6}$ | $194^{+5}_{-12}$ | 1.0 | $0.28^{+0.07}_{-0.17}$ | $0.06^{+0.02}_{-0.04}$ | 1.0 | 0.35 | 0.7 | 94.95 | Y |
| 3 | $102^{+0}_{0}$ | $102^{+0}_{0}$ | $204^{+0}_{0}$ | 1.0 | $0.36^{+0.0}_{0.0}$ | $0.08^{+0.0}_{0.0}$ | 1.0 | 0.7 | 0.0 | 97.41 | Y |
| 4 | $103^{+0}_{0}$ | $103^{+0}_{0}$ | $206^{+0}_{-1}$ | 1.0 | $0.19^{+0.03}_{-0.0}$ | $0.04^{+0.01}_{-0.0}$ | 1.0 | 0.53 | 0.61 | 101.24 | Y |
| 5 | $101^{+6}_{-3}$ | $101^{+6}_{-3}$ | $202^{+11}_{-7}$ | 1.0 | $0.18^{+0.14}_{-0.07}$ | $0.04^{+0.03}_{-0.02}$ | 1.0 | 0.53 | 0.61 | 100.39 | N |
| 6 | $82^{+6}_{-5}$ | $82^{+6}_{-5}$ | $165^{+11}_{-9}$ | 1.0 | $0.74^{+0.23}_{-0.32}$ | $0.15^{+0.04}_{-0.06}$ | 1.0 | $-0.0$ | 0.61 | 89.19 | Y |
| 7 | $99^{+11}_{-11}$ | $99^{+11}_{-11}$ | $198^{+21}_{-21}$ | 1.0 | $0.07^{+0.13}_{-0.06}$ | $0.02^{+0.03}_{-0.01}$ | 1.0 | 0.18 | 0.7 | 96.42 | Y |
| 8 | $101^{+4}_{-7}$ | $101^{+4}_{-7}$ | $201^{+9}_{-15}$ | 1.0 | $0.18^{+0.14}_{-0.1}$ | $0.04^{+0.03}_{-0.02}$ | 1.0 | 0.42 | 0.67 | 99.39 | N |
| 9 | $95^{+3}_{0}$ | $95^{+3}_{0}$ | $190^{+5}_{0}$ | 1.0 | $0.25^{+0.13}_{-0.01}$ | $0.06^{+0.03}_{-0.0}$ | 1.0 | 0.23 | 0.7 | 95.08 | N |
| 10 | $82^{+7}_{-4}$ | $82^{+7}_{-4}$ | $163^{+14}_{-8}$ | 1.0 | $0.77^{+0.25}_{-0.29}$ | $0.16^{+0.05}_{-0.06}$ | 1.0 | $-0.0$ | 0.0 | 83.97 | Y |

| | | | | | | | | | | | | |
|---|---|---|---|---|---|---|---|---|---|---|---|---|
| 11 | $106^{+0}_{-6}$ | $106^{+0}_{-6}$ | $211^{+0}_{-13}$ | 1.0 | $0.07^{+0.23}_{0.0}$ | $0.02^{+0.05}_{0.0}$ | 1.0 | 0.35 | 0.7 | 97.75 | Y |
| 12 | $103^{+5}_{-14}$ | $103^{+5}_{-14}$ | $207^{+10}_{-27}$ | 1.0 | $0.11^{+0.12}_{-0.05}$ | $0.03^{+0.03}_{-0.01}$ | 1.0 | 0.37 | 0.7 | 99.76 | Y |
| **Precessing eBBH runs** | | | | | | | | | | | |
| 1 | $81^{+7}_{-6}$ | $61^{+5}_{-5}$ | $142^{+12}_{-11}$ | 0.75 | $6.33^{+1.18}_{-1.42}$ | $0.97^{+0.19}_{-0.13}$ | 0.0 | $-0.0$ | 0.53 | 100.24 | Y |
| 2 | $93^{+12}_{-15}$ | $62^{+8}_{-10}$ | $156^{+19}_{-25}$ | 0.67 | $4.68^{+2.11}_{-1.48}$ | $0.76^{+0.27}_{-0.2}$ | 0.0 | 0.02 | 0.8 | 101.47 | Y |
| 3 | $81^{+15}_{-6}$ | $66^{+12}_{-5}$ | $147^{+26}_{-12}$ | 0.82 | $5.56^{+1.01}_{-2.31}$ | $0.87^{+0.13}_{-0.31}$ | 0.0 | 0.01 | 0.8 | 102.27 | Y |
| 4 | $74^{+11}_{-10}$ | $74^{+11}_{-10}$ | $148^{+21}_{-20}$ | 1.0 | $5.28^{+1.57}_{-2.16}$ | $0.83^{+0.2}_{-0.29}$ | 0.0 | 0.01 | 0.8 | 101.93 | N |
| 5 | $65^{+8}_{-6}$ | $65^{+8}_{-6}$ | $130^{+16}_{-12}$ | 1.0 | $7.6^{+1.34}_{-1.8}$ | $1.12^{+0.16}_{-0.22}$ | 0.0 | 0.0 | 0.78 | 101.5 | Y |
| 6 | $86^{+4}_{-10}$ | $86^{+4}_{-10}$ | $172^{+8}_{-19}$ | 1.0 | $3.71^{+0.78}_{-1.28}$ | $0.62^{+0.11}_{-0.18}$ | 0.26 | 0.0 | 0.7 | 102.23 | N |
| 7 | $87^{+15}_{-9}$ | $87^{+15}_{-9}$ | $174^{+30}_{-19}$ | 1.0 | $3.44^{+1.41}_{-1.51}$ | $0.59^{+0.19}_{-0.22}$ | 0.33 | 0.0 | 0.7 | 101.87 | N |
| 8 | $82^{+14}_{-10}$ | $82^{+14}_{-10}$ | $163^{+27}_{-20}$ | 1.0 | $4.15^{+1.75}_{-1.68}$ | $0.69^{+0.23}_{-0.24}$ | 0.4 | 0.0 | 0.7 | 97.59 | Y |
| 9 | $109^{+0}_{-16}$ | $109^{+0}_{-16}$ | $218^{+0}_{-32}$ | 1.0 | $1.21^{+1.29}_{0.0}$ | $0.24^{+0.21}_{0.0}$ | 0.46 | 0.0 | 0.7 | 97.37 | N |
| 10 | $79^{+13}_{-11}$ | $79^{+13}_{-11}$ | $159^{+27}_{-22}$ | 1.0 | $4.41^{+1.97}_{-2.05}$ | $0.72^{+0.25}_{-0.29}$ | 0.52 | 0.0 | 0.7 | 98.58 | Y |
| 11 | $81^{+5}_{-9}$ | $81^{+5}_{-9}$ | $162^{+11}_{-18}$ | 1.0 | $5.21^{+1.01}_{-1.31}$ | $0.82^{+0.13}_{-0.17}$ | 0.57 | 0.0 | 0.7 | 105.32 | N |
| 12 | $102^{+7}_{-16}$ | $102^{+7}_{-16}$ | $204^{+14}_{-33}$ | 1.0 | $1.84^{+1.07}_{-0.54}$ | $0.35^{+0.16}_{-0.09}$ | 0.67 | 0.0 | 0.7 | 107.91 | Y |
| 13 | $104^{+4}_{-5}$ | $104^{+4}_{-5}$ | $209^{+8}_{-10}$ | 1.0 | $0.53^{+0.2}_{-0.15}$ | $0.11^{+0.04}_{-0.03}$ | 0.86 | 0.0 | 0.7 | 103.52 | Y |
| 14 | $115^{+0}_{-4}$ | $115^{+0}_{-4}$ | $229^{+0}_{-9}$ | 1.0 | $0.11^{+0.03}_{0.0}$ | $0.03^{+0.01}_{0.0}$ | 0.95 | 0.0 | 0.7 | 100.64 | N |
| 15 | $80^{+15}_{-4}$ | $80^{+15}_{-4}$ | $160^{+31}_{-8}$ | 1.0 | $5.04^{+0.75}_{-2.03}$ | $0.8^{+0.1}_{-0.28}$ | 0.57 | 0.0 | 0.7 | 105.83 | N |
| 16 | $80^{+12}_{-9}$ | $80^{+12}_{-9}$ | $159^{+24}_{-18}$ | 1.0 | $4.69^{+1.41}_{-1.65}$ | $0.76^{+0.18}_{-0.23}$ | 0.57 | 0.0 | 0.7 | 106.22 | Y |
| 17 | $71^{+16}_{-3}$ | $71^{+16}_{-3}$ | $143^{+33}_{-7}$ | 1.0 | $5.99^{+0.43}_{-2.92}$ | $0.92^{+0.05}_{-0.39}$ | 0.57 | 0.0 | 0.7 | 104.97 | Y |
| 18 | $70^{+9}_{-8}$ | $70^{+9}_{-8}$ | $139^{+19}_{-15}$ | 1.0 | $6.3^{+1.89}_{-1.72}$ | $0.96^{+0.23}_{-0.22}$ | 0.57 | 0.0 | 0.7 | 103.5 | Y |
| 19 | $74^{+9}_{-5}$ | $74^{+9}_{-5}$ | $149^{+17}_{-10}$ | 1.0 | $5.11^{+1.01}_{-1.36}$ | $0.81^{+0.13}_{-0.18}$ | 0.26 | 0.0 | 0.7 | 98.21 | N |
| 20 | $72^{+7}_{-3}$ | $72^{+7}_{-3}$ | $144^{+14}_{-6}$ | 1.0 | $5.63^{+0.65}_{-1.4}$ | $0.88^{+0.08}_{-0.18}$ | 0.33 | 0.0 | 0.7 | 99.77 | Y |
| 21 | $72^{+8}_{-11}$ | $72^{+8}_{-11}$ | $145^{+15}_{-23}$ | 1.0 | $5.28^{+1.78}_{-1.62}$ | $0.83^{+0.26}_{-0.18}$ | 0.4 | 0.0 | 0.7 | 97.25 | N |
| 22 | $64^{+7}_{-5}$ | $64^{+7}_{-5}$ | $128^{+14}_{-11}$ | 1.0 | $6.98^{+1.2}_{-1.69}$ | $1.05^{+0.14}_{-0.21}$ | 0.46 | 0.0 | 0.7 | 94.44 | N |
| 23 | $72^{+7}_{-6}$ | $72^{+7}_{-6}$ | $144^{+15}_{-13}$ | 1.0 | $5.9^{+1.31}_{-1.37}$ | $0.91^{+0.16}_{-0.17}$ | 0.52 | 0.0 | 0.7 | 100.81 | N |
| 24 | $70^{+8}_{-7}$ | $70^{+8}_{-7}$ | $140^{+15}_{-14}$ | 1.0 | $6.15^{+1.63}_{-1.57}$ | $0.94^{+0.2}_{-0.2}$ | 0.57 | 0.0 | 0.7 | 102.63 | Y |
| 25 | $88^{+12}_{-11}$ | $88^{+12}_{-11}$ | $177^{+24}_{-23}$ | 1.0 | $2.43^{+1.38}_{-0.9}$ | $0.44^{+0.2}_{-0.14}$ | 0.67 | 0.0 | 0.7 | 101.72 | N |
| 26 | $100^{+3}_{-12}$ | $100^{+3}_{-12}$ | $200^{+7}_{-24}$ | 1.0 | $0.57^{+0.4}_{-0.34}$ | $0.12^{+0.08}_{-0.07}$ | 0.86 | 0.0 | 0.7 | 98.77 | N |
| 27 | $88^{+0}_{0}$ | $88^{+0}_{0}$ | $176^{+0}_{0}$ | 1.0 | $0.66^{+0.0}_{0.0}$ | $0.14^{+0.0}_{0.0}$ | 0.95 | 0.0 | 0.7 | 96.25 | N |
| 28 | $79^{+21}_{-8}$ | $79^{+21}_{-8}$ | $159^{+42}_{-15}$ | 1.0 | $4.51^{+1.43}_{-2.67}$ | $0.73^{+0.18}_{-0.39}$ | 0.57 | 0.0 | 0.7 | 105.65 | N |
| 29 | $76^{+7}_{-5}$ | $76^{+7}_{-5}$ | $152^{+14}_{-10}$ | 1.0 | $7.76^{+1.24}_{-1.12}$ | $1.14^{+0.15}_{-0.13}$ | 0.0 | 0.6 | 0.77 | 100.04 | N |
| **Aligned eBBH runs** | | | | | | | | | | | |
| 1 | $72^{+11}_{-9}$ | $36^{+6}_{-5}$ | $108^{+17}_{-14}$ | 0.5 | $5.58^{+2.06}_{-3.11}$ | $0.87^{+0.25}_{-0.43}$ | 0.57 | 0.8 | 0.0 | 65.56 | Y |
| 2 | $101^{+12}_{-7}$ | $51^{+6}_{-4}$ | $152^{+18}_{-11}$ | 0.5 | $7.69^{+1.1}_{-1.27}$ | $1.13^{+0.13}_{-0.15}$ | 0.57 | 0.67 | 0.0 | 91.17 | Y |
| 3 | $52^{+7}_{-10}$ | $26^{+3}_{-5}$ | $78^{+10}_{-15}$ | 0.5 | $3.45^{+3.02}_{-1.22}$ | $0.59^{+0.39}_{-0.18}$ | 0.57 | 0.53 | 0.0 | 46.52 | Y |
| 4 | $83^{+7}_{-9}$ | $42^{+4}_{-4}$ | $125^{+11}_{-13}$ | 0.5 | $7.05^{+1.64}_{-1.11}$ | $1.05^{+0.19}_{-0.14}$ | 0.57 | 0.4 | 0.0 | 79.74 | N |
| 5 | $75^{+10}_{-12}$ | $37^{+5}_{-6}$ | $112^{+15}_{-18}$ | 0.5 | $5.75^{+2.09}_{-1.42}$ | $0.89^{+0.25}_{-0.18}$ | 0.57 | 0.53 | 0.0 | 72.93 | Y |
| 6 | $91^{+9}_{-6}$ | $45^{+4}_{-3}$ | $136^{+13}_{-9}$ | 0.5 | $7.03^{+1.19}_{-1.46}$ | $1.05^{+0.14}_{-0.18}$ | 0.57 | 0.4 | 0.0 | 98.57 | Y |
| 7 | $95^{+10}_{-2}$ | $47^{+5}_{-1}$ | $142^{+15}_{-3}$ | 0.5 | $6.56^{+0.36}_{-1.39}$ | $0.99^{+0.05}_{-0.17}$ | 0.57 | 0.27 | 0.0 | 102.33 | Y |
| 8 | $100^{+5}_{-10}$ | $50^{+3}_{-5}$ | $150^{+8}_{-14}$ | 0.5 | $4.78^{+1.16}_{-0.71}$ | $0.77^{+0.15}_{-0.09}$ | 0.57 | 0.27 | 0.0 | 102.89 | Y |
| 9 | $93^{+7}_{-4}$ | $47^{+3}_{-2}$ | $140^{+10}_{-6}$ | 0.5 | $7.82^{+0.78}_{-1.16}$ | $1.15^{+0.09}_{-0.14}$ | 0.57 | 0.27 | 0.0 | 98.8 | N |
| 10 | $98^{+8}_{-3}$ | $49^{+4}_{-1}$ | $147^{+12}_{-4}$ | 0.5 | $5.72^{+0.19}_{-1.21}$ | $0.89^{+0.02}_{-0.16}$ | 0.57 | 0.13 | 0.0 | 102.95 | Y |
| 11 | $104^{+5}_{-10}$ | $52^{+2}_{-5}$ | $156^{+7}_{-15}$ | 0.5 | $3.99^{+0.88}_{-0.77}$ | $0.66^{+0.12}_{-0.11}$ | 0.57 | 0.13 | 0.0 | 103.72 | N |
| 12 | $108^{+9}_{-9}$ | $54^{+5}_{-4}$ | $162^{+14}_{-13}$ | 0.5 | $2.48^{+1.22}_{-0.56}$ | $0.45^{+0.18}_{-0.09}$ | 0.57 | 0.0 | 0.0 | 101.59 | Y |
| 13 | $171^{+7}_{-6}$ | $43^{+2}_{-1}$ | $214^{+9}_{-7}$ | 0.25 | $0.22^{+0.08}_{-0.09}$ | $0.05^{+0.02}_{-0.02}$ | 0.99 | 0.64 | 0.0 | 102.47 | N |
| 14 | $157^{+6}_{-16}$ | $52^{+2}_{-5}$ | $210^{+8}_{-21}$ | 0.33 | $0.21^{+0.19}_{-0.08}$ | $0.05^{+0.04}_{-0.02}$ | 0.99 | 0.6 | 0.0 | 102.71 | N |
| **Anti-aligned eBBH runs** | | | | | | | | | | | |
| 1 | $102^{+7}_{-6}$ | $51^{+3}_{-3}$ | $153^{+10}_{-9}$ | 0.5 | $4.85^{+0.64}_{-0.97}$ | $0.78^{+0.08}_{-0.13}$ | 0.57 | $-0.0$ | 0.0 | 102.59 | Y |
| 2 | $101^{+8}_{-4}$ | $51^{+4}_{-2}$ | $152^{+12}_{-5}$ | 0.5 | $3.5^{+0.42}_{-0.84}$ | $0.6^{+0.06}_{-0.12}$ | 0.57 | $-0.13$ | 0.0 | 101.09 | N |
| 3 | $106^{+6}_{-11}$ | $53^{+3}_{-5}$ | $159^{+9}_{-16}$ | 0.5 | $2.73^{+0.66}_{-0.78}$ | $0.48^{+0.1}_{-0.12}$ | 0.57 | $-0.13$ | 0.0 | 100.77 | N |
| 4 | $103^{+6}_{-3}$ | $51^{+3}_{-2}$ | $154^{+8}_{-5}$ | 0.5 | $3.13^{+0.53}_{-0.43}$ | $0.54^{+0.08}_{-0.06}$ | 0.57 | $-0.27$ | 0.0 | 100.03 | N |
| 5 | $105^{+7}_{-7}$ | $53^{+3}_{-4}$ | $158^{+10}_{-11}$ | 0.5 | $2.46^{+0.97}_{-0.65}$ | $0.44^{+0.14}_{-0.1}$ | 0.57 | $-0.27$ | 0.0 | 100.32 | N |
| 6 | $108^{+7}_{-8}$ | $54^{+4}_{-4}$ | $163^{+11}_{-13}$ | 0.5 | $1.83^{+0.59}_{-0.63}$ | $0.35^{+0.09}_{-0.11}$ | 0.57 | $-0.27$ | 0.0 | 100.94 | N |
| 7 | $98^{+11}_{0}$ | $49^{+6}_{0}$ | $147^{+17}_{0}$ | 0.5 | $2.58^{+0.34}_{-0.66}$ | $0.46^{+0.05}_{-0.1}$ | 0.57 | $-0.4$ | 0.0 | 98.42 | N |
| 8 | $109^{+4}_{-10}$ | $54^{+2}_{-5}$ | $163^{+5}_{-15}$ | 0.5 | $1.58^{+0.63}_{-0.68}$ | $0.31^{+0.1}_{-0.12}$ | 0.57 | $-0.4$ | 0.0 | 98.83 | N |
| 9 | $110^{+7}_{-8}$ | $28^{+2}_{-2}$ | $138^{+9}_{-10}$ | 0.25 | $1.57^{+0.47}_{-0.44}$ | $0.3^{+0.08}_{-0.08}$ | 0.43 | $-0.64$ | 0.0 | 97.1 | N |
| 10 | $114^{+7}_{-8}$ | $28^{+2}_{-2}$ | $142^{+8}_{-10}$ | 0.25 | $1.56^{+0.23}_{-0.66}$ | $0.3^{+0.04}_{-0.12}$ | 0.46 | $-0.64$ | 0.0 | 97.01 | N |

| | | | | | | | | | | | |
|---|---|---|---|---|---|---|---|---|---|---|---|
| 11 | $123^{+2}_{-15}$ | $31^{+1}_{-4}$ | $154^{+3}_{-18}$ | 0.25 | $1.18^{+0.53}_{-0.18}$ | $0.24^{+0.09}_{-0.03}$ | 0.5 | $-0.64$ | 0.0 | 95.73 | N |
| 12 | $122^{+15}_{-7}$ | $30^{+4}_{-2}$ | $152^{+18}_{-9}$ | 0.25 | $1.05^{+0.46}_{-0.36}$ | $0.21^{+0.08}_{-0.07}$ | 0.52 | $-0.64$ | 0.0 | 96.1 | N |
| 13 | $118^{+8}_{0}$ | $30^{+2}_{0}$ | $148^{+10}_{0}$ | 0.25 | $1.07^{+0.13}_{-0.12}$ | $0.22^{+0.02}_{-0.02}$ | 0.55 | $-0.64$ | 0.0 | 94.83 | N |
| 14 | $122^{+12}_{-5}$ | $30^{+3}_{-1}$ | $152^{+14}_{-6}$ | 0.25 | $0.88^{+0.42}_{-0.26}$ | $0.18^{+0.08}_{-0.05}$ | 0.57 | $-0.64$ | 0.0 | 95.21 | N |
| 15 | $126^{+9}_{-8}$ | $31^{+2}_{-2}$ | $157^{+11}_{-10}$ | 0.25 | $0.89^{+0.25}_{-0.34}$ | $0.18^{+0.05}_{-0.06}$ | 0.59 | $-0.64$ | 0.0 | 93.92 | N |
| 16 | $125^{+8}_{-9}$ | $31^{+2}_{-2}$ | $157^{+10}_{-11}$ | 0.25 | $0.81^{+0.25}_{-0.33}$ | $0.17^{+0.05}_{-0.06}$ | 0.62 | $-0.64$ | 0.0 | 93.09 | Y |
| 17 | $133^{+3}_{-8}$ | $33^{+1}_{-2}$ | $166^{+3}_{-11}$ | 0.25 | $0.57^{+0.0}_{-0.08}$ | $0.12^{+0.0}_{-0.02}$ | 0.67 | $-0.64$ | 0.0 | 91.1 | N |
| 18 | $127^{+6}_{-6}$ | $32^{+1}_{-1}$ | $159^{+7}_{-7}$ | 0.25 | $0.45^{+0.25}_{-0.02}$ | $0.1^{+0.05}_{-0.0}$ | 0.71 | $-0.64$ | 0.0 | 89.76 | N |
| 19 | $129^{+10}_{-8}$ | $32^{+3}_{-2}$ | $161^{+13}_{-11}$ | 0.25 | $0.52^{+0.24}_{-0.2}$ | $0.11^{+0.05}_{-0.04}$ | 0.75 | $-0.64$ | 0.0 | 88.43 | N |
| 20 | $127^{+9}_{-4}$ | $32^{+2}_{-1}$ | $158^{+11}_{-6}$ | 0.25 | $0.48^{+0.02}_{-0.23}$ | $0.1^{+0.0}_{-0.05}$ | 0.79 | $-0.64$ | 0.0 | 87.85 | N |
| 21 | $134^{+5}_{-8}$ | $33^{+1}_{-2}$ | $167^{+7}_{-10}$ | 0.25 | $0.33^{+0.24}_{-0.16}$ | $0.07^{+0.05}_{-0.03}$ | 0.82 | $-0.64$ | 0.0 | 87.94 | N |
| 22 | $129^{+8}_{-3}$ | $32^{+2}_{-1}$ | $161^{+10}_{-4}$ | 0.25 | $0.26^{+0.16}_{-0.09}$ | $0.06^{+0.03}_{-0.02}$ | 0.86 | $-0.64$ | 0.0 | 86.47 | N |
| 23 | $128^{+6}_{-4}$ | $32^{+1}_{-1}$ | $160^{+7}_{-5}$ | 0.25 | $0.27^{+0.12}_{-0.02}$ | $0.06^{+0.02}_{-0.0}$ | 0.89 | $-0.64$ | 0.0 | 86.96 | N |
| 24 | $135^{+8}_{0}$ | $34^{+2}_{0}$ | $169^{+10}_{0}$ | 0.25 | $0.17^{+0.09}_{-0.0}$ | $0.04^{+0.02}_{-0.0}$ | 0.95 | $-0.64$ | 0.0 | 93.94 | N |
| 25 | $153^{+24}_{-9}$ | $38^{+6}_{-2}$ | $191^{+30}_{-12}$ | 0.25 | $0.2^{+0.03}_{-0.1}$ | $0.05^{+0.01}_{-0.02}$ | 0.96 | $-0.64$ | 0.0 | 97.76 | N |
| 26 | $172^{+17}_{-7}$ | $43^{+4}_{-2}$ | $215^{+21}_{-9}$ | 0.25 | $0.19^{+0.08}_{-0.1}$ | $0.04^{+0.02}_{-0.02}$ | 0.98 | $-0.64$ | 0.0 | 100.44 | Y |
| 27 | $99^{+10}_{-10}$ | $33^{+3}_{-3}$ | $132^{+13}_{-13}$ | 0.33 | $2.1^{+0.8}_{-0.56}$ | $0.39^{+0.12}_{-0.09}$ | 0.4 | $-0.6$ | 0.0 | 83.57 | N |
| 28 | $102^{+8}_{-9}$ | $34^{+3}_{-3}$ | $136^{+10}_{-12}$ | 0.33 | $2.19^{+0.58}_{-0.7}$ | $0.4^{+0.09}_{-0.11}$ | 0.43 | $-0.6$ | 0.0 | 98.76 | N |
| 29 | $109^{+7}_{-8}$ | $36^{+2}_{-3}$ | $146^{+10}_{-11}$ | 0.33 | $1.79^{+0.64}_{-0.56}$ | $0.34^{+0.1}_{-0.1}$ | 0.46 | $-0.6$ | 0.0 | 98.45 | N |
| 30 | $111^{+9}_{-7}$ | $37^{+3}_{-2}$ | $148^{+12}_{-9}$ | 0.33 | $1.7^{+0.48}_{-0.75}$ | $0.32^{+0.08}_{-0.13}$ | 0.5 | $-0.6$ | 0.0 | 97.27 | N |
| 31 | $109^{+1}_{-1}$ | $36^{+0}_{0}$ | $145^{+1}_{-1}$ | 0.33 | $2.06^{+0.03}_{-0.18}$ | $0.38^{+0.0}_{-0.03}$ | 0.52 | $-0.6$ | 0.0 | 96.6 | N |
| 32 | $116^{+9}_{-5}$ | $39^{+3}_{-2}$ | $154^{+12}_{-7}$ | 0.33 | $1.52^{+0.0}_{-0.67}$ | $0.29^{+0.0}_{-0.12}$ | 0.57 | $-0.6$ | 0.0 | 95.29 | N |
| 33 | $111^{+12}_{-2}$ | $37^{+4}_{-1}$ | $148^{+16}_{-2}$ | 0.33 | $1.06^{+0.5}_{-0.15}$ | $0.22^{+0.09}_{-0.03}$ | 0.59 | $-0.6$ | 0.0 | 95.39 | N |
| 34 | $119^{+9}_{-9}$ | $40^{+3}_{-3}$ | $158^{+11}_{-12}$ | 0.33 | $1.08^{+0.36}_{-0.46}$ | $0.22^{+0.06}_{-0.09}$ | 0.62 | $-0.6$ | 0.0 | 94.42 | N |
| 35 | $120^{+9}_{-9}$ | $40^{+3}_{-3}$ | $160^{+12}_{-12}$ | 0.33 | $0.92^{+0.32}_{-0.36}$ | $0.19^{+0.06}_{-0.07}$ | 0.67 | $-0.6$ | 0.0 | 92.39 | N |
| 36 | $123^{+9}_{-8}$ | $41^{+3}_{-3}$ | $163^{+11}_{-10}$ | 0.33 | $0.63^{+0.29}_{-0.15}$ | $0.13^{+0.06}_{-0.02}$ | 0.71 | $-0.6$ | 0.0 | 91.97 | N |
| 37 | $126^{+9}_{-10}$ | $42^{+3}_{-3}$ | $168^{+12}_{-13}$ | 0.33 | $0.53^{+0.33}_{-0.11}$ | $0.11^{+0.06}_{-0.02}$ | 0.75 | $-0.6$ | 0.0 | 89.91 | N |
| 38 | $124^{+9}_{-8}$ | $41^{+3}_{-3}$ | $166^{+12}_{-11}$ | 0.33 | $0.53^{+0.23}_{-0.22}$ | $0.12^{+0.05}_{-0.04}$ | 0.79 | $-0.6$ | 0.0 | 89.6 | N |
| 39 | $125^{+8}_{-7}$ | $42^{+3}_{-2}$ | $167^{+11}_{-10}$ | 0.33 | $0.5^{+0.11}_{-0.26}$ | $0.11^{+0.02}_{-0.05}$ | 0.82 | $-0.6$ | 0.0 | 87.92 | N |
| 40 | $126^{+5}_{-9}$ | $42^{+2}_{-3}$ | $168^{+7}_{-12}$ | 0.33 | $0.38^{+0.13}_{-0.22}$ | $0.08^{+0.03}_{-0.04}$ | 0.86 | $-0.6$ | 0.0 | 86.69 | N |
| 41 | $126^{+5}_{-6}$ | $42^{+2}_{-2}$ | $167^{+6}_{-9}$ | 0.33 | $0.29^{+0.18}_{-0.14}$ | $0.06^{+0.04}_{-0.03}$ | 0.89 | $-0.6$ | 0.0 | 86.64 | N |
| 42 | $131^{+4}_{-4}$ | $44^{+1}_{-1}$ | $175^{+5}_{-5}$ | 0.33 | $0.17^{+0.12}_{-0.06}$ | $0.04^{+0.03}_{-0.01}$ | 0.95 | $-0.6$ | 0.0 | 94.91 | Y |
| 43 | $139^{+27}_{-7}$ | $47^{+9}_{-2}$ | $186^{+36}_{-9}$ | 0.33 | $0.18^{+0.11}_{-0.12}$ | $0.04^{+0.02}_{-0.03}$ | 0.96 | $-0.6$ | 0.0 | 99.14 | N |
| 44 | $157^{+2}_{-18}$ | $52^{+1}_{-6}$ | $210^{+3}_{-24}$ | 0.33 | $0.22^{+0.02}_{-0.11}$ | $0.05^{+0.0}_{-0.02}$ | 0.98 | $-0.6$ | 0.0 | 100.91 | Y |
| 45 | $107^{+9}_{-10}$ | $53^{+4}_{-5}$ | $160^{+13}_{-15}$ | 0.5 | $1.65^{+0.96}_{-0.58}$ | $0.32^{+0.15}_{-0.1}$ | 0.57 | $-0.53$ | 0.0 | 97.8 | N |
| 46 | $95^{+7}_{-9}$ | $48^{+3}_{-5}$ | $143^{+10}_{-14}$ | 0.5 | $2.88^{+1.08}_{-0.9}$ | $0.51^{+0.15}_{-0.14}$ | 0.46 | $-0.53$ | 0.0 | 100.05 | N |
| 47 | $103^{+9}_{-7}$ | $52^{+5}_{-4}$ | $155^{+14}_{-11}$ | 0.5 | $1.71^{+0.65}_{-0.68}$ | $0.33^{+0.1}_{-0.12}$ | 0.57 | $-0.53$ | 0.0 | 97.96 | N |
| 48 | $109^{+0}_{-7}$ | $54^{+0}_{-4}$ | $163^{+0}_{-11}$ | 0.5 | $1.14^{+0.73}_{0.0}$ | $0.23^{+0.12}_{0.0}$ | 0.62 | $-0.53$ | 0.0 | 96.71 | N |
| 49 | $112^{+9}_{-9}$ | $56^{+5}_{-5}$ | $168^{+14}_{-14}$ | 0.5 | $0.97^{+0.57}_{-0.28}$ | $0.2^{+0.1}_{-0.05}$ | 0.67 | $-0.53$ | 0.0 | 95.08 | N |
| 50 | $110^{+9}_{-7}$ | $55^{+5}_{-3}$ | $164^{+14}_{-10}$ | 0.5 | $0.84^{+0.32}_{-0.32}$ | $0.17^{+0.06}_{-0.06}$ | 0.75 | $-0.53$ | 0.0 | 92.5 | N |
| 51 | $115^{+8}_{-11}$ | $57^{+4}_{-5}$ | $172^{+12}_{-16}$ | 0.5 | $0.47^{+0.51}_{-0.19}$ | $0.1^{+0.1}_{-0.04}$ | 0.82 | $-0.53$ | 0.0 | 89.57 | N |
| 52 | $107^{+2}_{-9}$ | $54^{+1}_{-5}$ | $161^{+4}_{-14}$ | 0.5 | $1.95^{+0.94}_{-0.12}$ | $0.37^{+0.14}_{-0.02}$ | 0.57 | $-0.53$ | 0.0 | 97.68 | N |
| 53 | $104^{+11}_{-6}$ | $52^{+6}_{-3}$ | $155^{+17}_{-8}$ | 0.5 | $1.83^{+0.43}_{-0.72}$ | $0.35^{+0.07}_{-0.12}$ | 0.57 | $-0.67$ | 0.0 | 96.21 | N |
| 54 | $103^{+8}_{-9}$ | $52^{+4}_{-4}$ | $155^{+12}_{-13}$ | 0.5 | $1.61^{+0.53}_{-0.58}$ | $0.31^{+0.09}_{-0.1}$ | 0.57 | $-0.8$ | 0.0 | 95.18 | N |

TABLE II: Details of selected source parameters of GW190521. Each parameter reported with median value with 90% C.L, that include statistical error and systematic error. Here we report total 325 estimation with different NR simulations. The columns show the source-frame primary mass $m_1$, source-frame secondary mass $m_2$, source frame total mass $M$, mass ratio $q$, luminosity distance $D$, redshift $z$, eccentricity $e$, dimensionless effective aligned spin $\chi_{eff}$, dimensionless dominant effective precession spin $\chi_p$, marginalized likelihood log $\mathcal{L}_{marg}$ and consistency for each estimation.